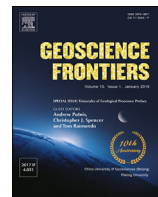


HOSTED BY  
Contents lists available at ScienceDirect

China University of Geosciences (Beijing)

**Geoscience Frontiers**journal homepage: [www.elsevier.com/locate/gsf](http://www.elsevier.com/locate/gsf)**Research Paper****Extensional collapse of the Gondwana orogen: Evidence from Cambrian mafic magmatism in the Trivandrum Block, southern India**Qiong-Yan Yang<sup>a</sup>, Sohini Ganguly<sup>b</sup>, E. Shaji<sup>d,\*</sup>, Yunpeng Dong<sup>c</sup>, V. Nanda-Kumar<sup>e</sup><sup>a</sup>*School of Earth Science and Resources, China University of Geosciences, Beijing 100083, China*<sup>b</sup>*Department of Earth Science, Goa University, Taleigao Plateau, Goa 403206, India*<sup>c</sup>*State Key Laboratory of Continental Dynamics, Department of Geology, Northwest University, Northern Taibai Str. 229, Xi'an 710069, China*<sup>d</sup>*Department of Geology, University of Kerala, Thiruvananthapuram 695581, Kerala, India*<sup>e</sup>*National Center for Earth Science Studies, Akkulam, Trivandrum, India***ARTICLE INFO****Article history:**

Received 5 July 2017

Received in revised form

28 November 2017

Accepted 2 December 2017

Available online 20 December 2017

Handling Editor: Sanghoon Kwon

**Keywords:**

Mafic dykes

Geochemistry

Zircon U–Pb geochronology

Post-collisional extension

Gondwana supercontinent

**ABSTRACT**

The assembly of Late Neoproterozoic–Cambrian supercontinent Gondwana involved prolonged subduction and accretion generating arc magmatic and accretionary complexes, culminating in collision and formation of high grade metamorphic orogens. Here we report evidence for mafic magmatism associated with post-collisional extension from a suite of gabbroic rocks in the Trivandrum Block of southern Indian Gondwana fragment. Our petrological and geochemical data on these gabbroic suite show that they are analogous to high Fe tholeiitic basalts with evolution of the parental melts dominantly controlled by fractional crystallization. They display enrichment of LILE and LREE and depletion of HFSE with negative anomalies at Zr–Hf and Ti corresponding to subduction zone magmatic regime. The tectonic affinity of the gabbros coupled with their geochemical features endorse a heterogeneous mantle source with collective melt contributions from sub-slab asthenospheric mantle upwelling through slab break-off and arc-related metasomatized mantle wedge, with magma emplacement in subduction to post-collisional intraplate settings. The high Nb contents and positive Nb–Ta anomalies of the rocks are attributed to inflow of asthenospheric melts containing ancient recycled subducted slab components and/or fusion of subducted slab materials owing to upwelling of hot asthenosphere. Zircon grains from the gabbros show magmatic crystallization texture with low U and Pb content. The LA-ICPMS analyses show  $^{206}\text{Pb}/^{238}\text{U}$  mean ages in the range of 507–494 Ma suggesting Cambrian mafic magmatism. The post-collisional mafic magmatism identified in our study provides new insights into mantle dynamics during the waning stage of the birth of a supercontinent.

© 2018, China University of Geosciences (Beijing) and Peking University. Production and hosting by Elsevier B.V. This is an open access article under the CC BY-NC-ND license (<http://creativecommons.org/licenses/by-nc-nd/4.0/>).

**1. Introduction**

Magmatism in post-collisional settings provides important information on mantle processes, crustal reworking, and crust–mantle interaction. The geodynamic processes associated with post-collisional tectonics include slab breakoff, lithospheric delamination and/or convective removal of the lithosphere (e.g. Kay and Kay, 1993; Davies and von Blanckenburg, 1995; Molnar et al., 1998). In the case of slab break-off which involves the detachment of high density oceanic slab from the continental lithosphere, magmatism propagates through extensional fractures

and is of limited extend, immediately following the collisional event (Davies and von Blanckenburg, 1995; Gerya et al., 2004; Dokuz, 2011). In convective removal, the lowermost part of the lithosphere coupled with the upper part of the lithospheric mantle sinks down triggering asthenospheric upwelling and generating mixed magmas from juvenile crust and subduction-modified lithospheric mantle (e.g. Houseman et al., 1981; Conrad and Molnar, 1999; Krystopowicz and Currie, 2013). The mantle upwelling and heat input result in lithospheric extension providing pathways for magma migration and emplacement. Gabbroic magmas are sourced from either asthenospheric mantle or lithospheric mantle with distinct geochemical features (McDonough, 1990; Lightfoot et al., 1993; Ewart et al., 1998; Sklyarov et al., 2003). Mafic dykes derived from mantle magmas undergo crystallization differentiation and contamination by the crustal materials both in the

\* Corresponding author.

E-mail address: [shajigeology@gmail.com](mailto:shajigeology@gmail.com) (E. Shaji).

Peer-review under responsibility of China University of Geosciences (Beijing).

magma chamber and during ascent (DePaolo, 1981) and provide important clues to a variety of geological processes and tectonic environments.

The assembly of the Gondwana supercontinent occurred during the latest Neoproterozoic–Cambrian and was preceded by a prolonged subduction-accretion history from early to late Neoproterozoic building extensive continental arcs, and culminating in the collisional amalgamation of continental fragments and accompanying high grade metamorphism that reached up to ultrahigh-temperature granulite facies conditions (e.g., Santosh

et al., 2009, 2017; Collins et al., 2014; He et al., 2016). Southern Peninsular India occupied the central part of the Gondwana supercontinent and preserves the records of the subduction-collision history associated with the birth of Gondwana. However, no detailed information is available from this region on the post-collisional magmatism.

In this study, we report a suite of gabbroic dykes and sills from the Trivandrum Block in the southern part of Peninsular India (Fig. 1) which provide important insights into the post-collisional extensional collapse of the Gondwana orogen and accompanying

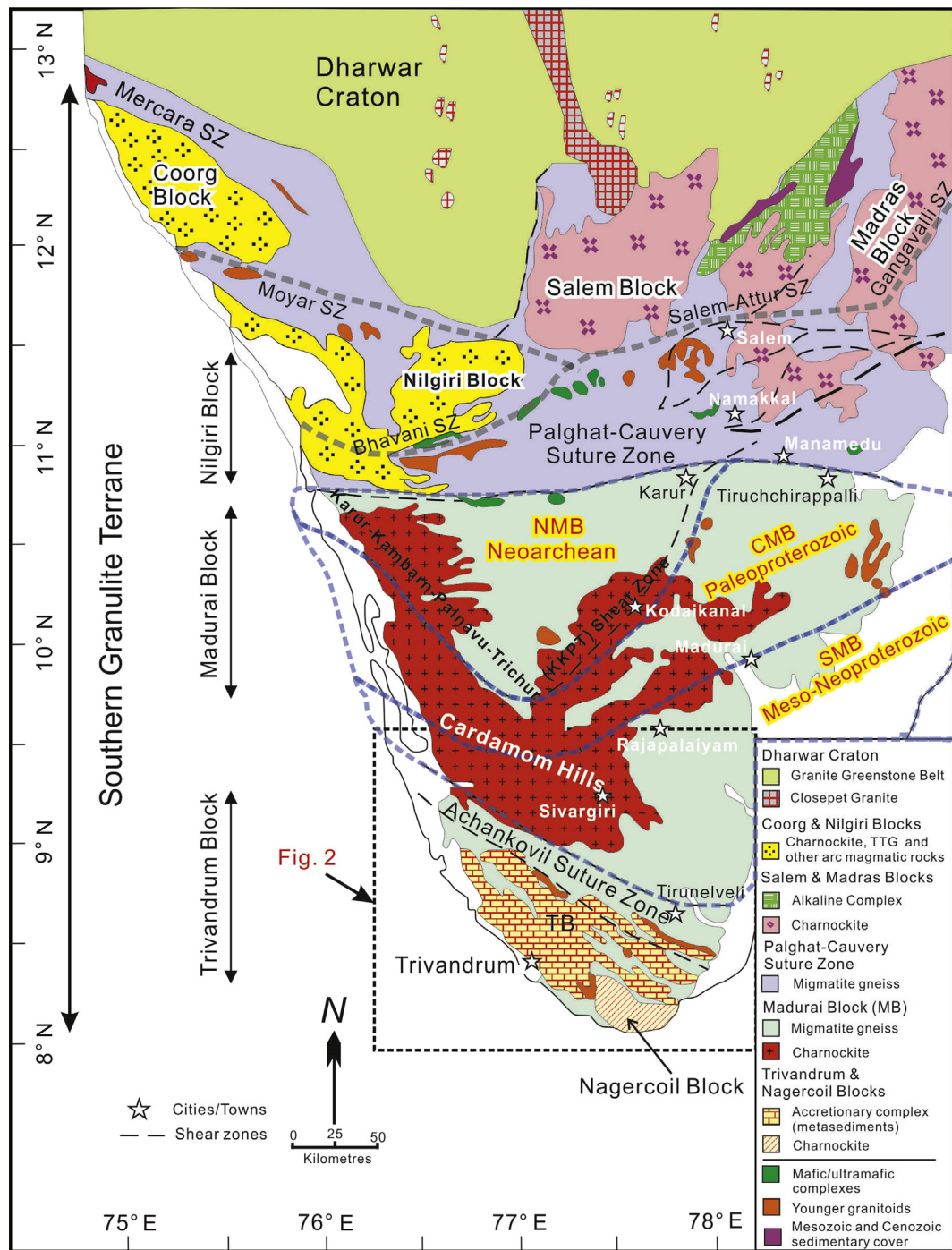


**Figure 1.** Generalized geological and tectonic framework of southern Peninsular India showing the major crustal blocks and intervening shear/suture zones (modified after Collins et al., 2014; Santosh et al., 2016, 2017).

mafic magmatism. We present petrologic, geochemical and zircon U-Pb geochronological data that indicate slab break-off and mantle upwelling leading to the formation and emplacement of mafic magmas within post-collisional setting.

## 2. Geological setting

The Southern Granulite Terrane (SGT) at the southern part of Peninsular India is a collage of crustal blocks varying in age from Mesoarchean through Neoarchean and Paleoproterozoic to late Neoproterozoic (Fig. 1; Collins et al., 2007, 2014; Clark et al., 2009, 2015; Santosh et al., 2009, 2016, 2017). These blocks were welded together at various times including Mesoarchean, Neoarchean and late Neoproterozoic–Cambrian along major suture zones, some of which are now represented by major transpressional shear zones (Chetty and Rao, 2006). The Trivandrum Block is located at the southern part of the SGT and is bound by the Achankovil shear/suture zone to the north and the Nagercoil Block to the south (Fig. 2). This crustal block is dominantly composed of granulite facies metasediments (khondalites represented by garnet-, sillimanite- and cordierite-bearing metapelites and leptynites represented by garnet-bearing felsic gneisses) interlayered with charnockites (orthopyroxene-bearing anhydrous granulites with or without garnet) and minor mafic granulites and calc-silicate rocks (Chacko et al., 1987; Santosh, 1987). Santosh et al. (2003) reported Archean–Paleoproterozoic detrital zircons from the metasediments of Trivandrum Block and late Neoproterozoic–Cambrian metamorphism. Collins et al. (2007) suggested that the protoliths of many of the metasedimentary gneisses in the Trivandrum Block were sourced from Paleoproterozoic and Neoarchean rocks which

were deposited later than 1900 Ma. Paleoproterozoic monazites were also identified from metasedimentary rocks of the Trivandrum Block in an earlier study (Bindu et al., 1998). Collins et al. (2007) correlated their source to Paleoproterozoic sedimentary rocks in central Madagascar and suggested that they both were sourced from the same East African rocks. Metamorphic zircon and monazite ages from the Trivandrum Block all cluster around late Neoproterozoic–Cambrian (Bindu et al., 1998; Santosh et al., 2003, 2006; Collins et al., 2007; Kröner et al., 2015, among others), correlated with tectonics associated with the final assembly of the Gondwana supercontinent. However, recent studies reveal that the basement rocks of the Trivandrum Block are mostly Paleoproterozoic (Kröner et al., 2015), with suspected multiple metamorphism both during late Paleoproterozoic and late Neoproterozoic–Cambrian (Liu et al., 2016; Harley and Nandakumar, 2016).

## 3. Sampling and petrography

This study focuses for the first time on the gabbroic rocks occurring as sills, dykes and boudinaged blocks within granulite facies metasediments (khondalites/leptynites) of the Trivandrum Block. The rock is dark-colored and fine-grained and is composed of equidimensional mosaic of xenomorphic grains. The width of these dykes and sills ranges from 10 cm to more than 1 m. The core of the mafic dykes/sills is generally fine grained and dark composed of clinopyroxene and plagioclase. Accessory minerals are mainly hornblende and magnetite. The rim domains of the dykes/sills in contact with metasedimentary host rocks additionally carry orthopyroxene and minor quartz and garnet. Chilled margins are

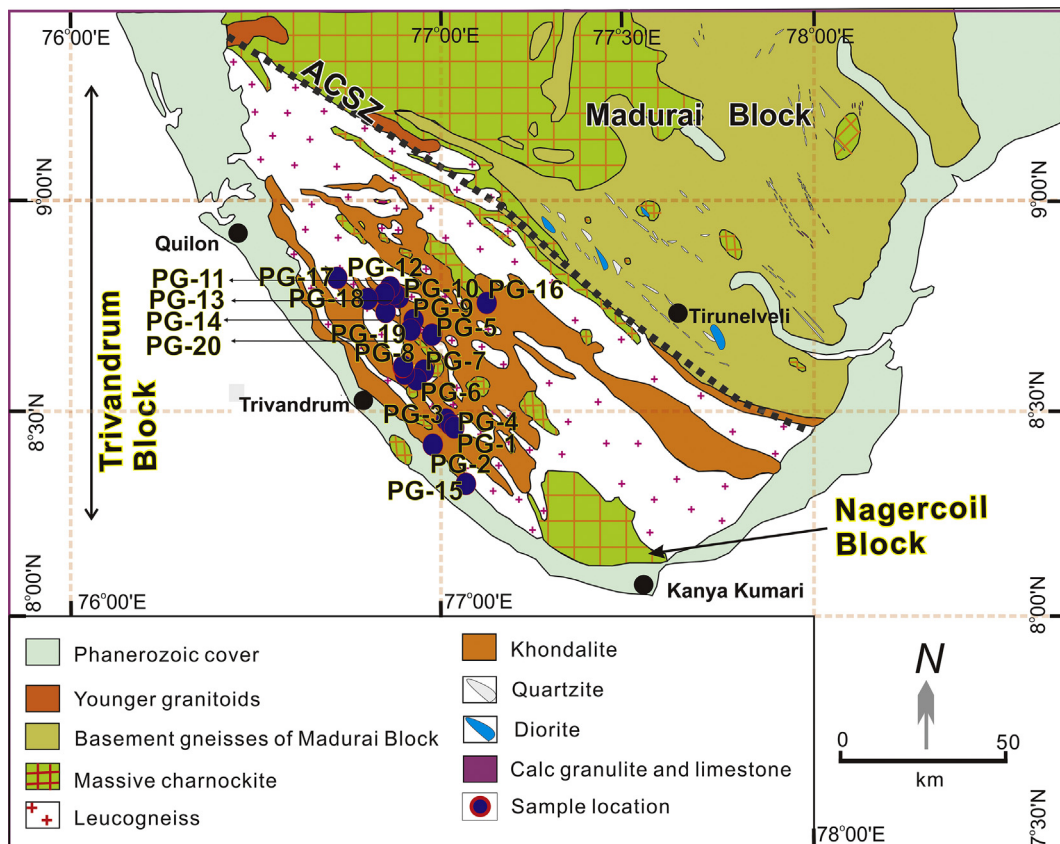


Figure 2. Geological framework of the southern part of the Madurai Block and the Trivandrum Block to the south showing sample locations of present study.

not distinctly observable and in some cases, the dykes/sills show minor gradational boundary, indicating that the surrounding rocks were still hot at the time of emplacement of the dykes/sills. The host metapelites carry cordierite, sillimanite and garnet along aluminous compositional bands or garnet and biotite in more psammitic varieties. Field relations suggest that the gabbroic dykes and sills intruded into the metapelitic rocks after the peak metamorphic event, although the host rocks and the mafic intrusions are co-folded and fractured in some localities indicating common late stage deformational history.

The representative localities investigated and sampled in this study are shown in Fig. 2 and a summary is given in Table 1. At Naruvamoodu (PG-1, Fig. 3a), a large quarry face exposes a series of closely spaced mafic sills (Fig. 3a) emplaced parallel to the compositional planes of the host metapelites. Gabbro dykes and sills occur as boudinaged layers and boudins within the gneissic units at several other localities in the Trivandrum block including Venjaramoodu (PG-20), Vattappara (PG-6), Chullalam (PG-5) and Kilimanoor (PG-12). Boulders and blocks of fine grained gabbroic rocks stand out in weathered and lateritised gneisses at Nagaroor (PG-13), Melattumuzhi (PG-9) and Kataikonam (PG-10). The host rocks are mainly khondalites (garnet-sillimanite-cordierite granulites), leptinites (felsic garnet gneisses with or without biotite) and

charnockites (orthopyroxene-bearing greasy green granulites with or without garnet).

Under thin section, the gabbroic rock is composed of interlocking grains of clinopyroxene and plagioclase with hornblende, magnetite and biotite as the major accessories and apatite and zircon as minor minerals (Fig. 4). Orthopyroxene, garnet and quartz occur toward the margin domains of the dykes/sills. The following mineral assemblages are identified: (1) Clinopyroxene + Plagioclase + Magnetite + Hornblende; (2) Clinopyroxene + Orthopyroxene + Plagioclase + Magnetite + Hornblende + Biotite; (3) Orthopyroxene + Clinopyroxene + Plagioclase + Garnet + Biotite + Magnetite + Quartz.

#### 4. Analytical techniques

##### 4.1. Whole rock geochemistry

Fresh samples of the gabbros were crushed using a jaw crusher and was fine powdered in an agate mortar. Major elements were analyzed at the National Geophysical Research Institute (NGRI), India by XRF (Phillips® MAGIX PRO Model 2440), with a relative standard deviation of <3% (Krishna et al., 2007). The sample powders were dissolved in reagent grade HF:HNO<sub>3</sub> acid mixture in Savillex screw top vessels for trace element analyses including rare earth (REE) and high field strength (HFS) elements. The analysis was performed using HR-ICP-MS (Nu ATTOM®, Nu Instruments, UK) at the National Geophysical Research Institute (NGRI), Hyderabad using <sup>103</sup>Rh as an internal standard. Replicate analyses of solution of standard G-2 (USGS) ensured drift correction and calibration. The precision and accuracy are better than RSD 5% for most of the trace elements, and RSD 10% in the case of HREE (Satyanarayanan et al., 2014). Anomalies of HFSE relative to neighboring REE are given as Nb/Nb\*, Zr/Zr\*, Hf/Hf\* and Ti/Ti\*. Mg# is calculated as Mg/(Mg + Fe<sup>T</sup>). The chondrite and primitive mantle normalization values are from Sun and McDonough (1989).

##### 4.2. Zircon U–Pb geochronology

Conventional heavy liquid and electro-magnetic techniques were employed for the separation of zircon grains from crushed rock samples, followed by handpicking and mounting in epoxy resin discs. The discs were then polished to expose the grains and carbon coated. Internal morphology of the zircons was examined using cathodoluminescence (CL). Zircon U–Pb analysis was carried out at National Key Laboratory of Continental Dynamics of Northwest University, by using laser ablation inductively coupled plasma spectrometry (LA-ICP-MS) following procedures given in Yuan et al. (2004). The laser spot diameter and frequency were 30 μm and 10 Hz, respectively. Zircon 91500 was employed as a standard and the standard silicate glass NIST was used to optimize the instrument. The raw data were processed using the GLITTER program to compute isotopic ratios and ages of <sup>207</sup>Pb/<sup>206</sup>Pb, <sup>206</sup>Pb/<sup>238</sup>U, and <sup>207</sup>Pb/<sup>235</sup>U. Data for common Pb was collected following the method outlined in Andersen (2002), and the ages were calculated by ISOPLOT 4.15 software (Ludwig, 2003).

#### 5. Geochemistry

##### 5.1. Major elements

Major and trace element compositions of thirteen mafic dykes/sills from Mukkunimala, Puvadakonam, Killiyoor, Chullalam, Vattappara, Mottakuzhi, Melattumuzhi, Ayiruppara, Nagaroor, Ozhukupara, Kattaikonam, Unnanpara, Venjaramudu, and Aramthanam are presented in Table 1. The chemical composition of the samples is plotted in terms of major element oxides in Fig. 5. The samples are enriched in MgO, CaO, MnO, and TiO<sub>2</sub> and depleted in Na<sub>2</sub>O, K<sub>2</sub>O, P<sub>2</sub>O<sub>5</sub>, and SiO<sub>2</sub>. The samples are plotted in the TAS diagram (Fig. 6) and are found to fall in the field of alkali basalts.

**Table 1**

Sample details analyzed for petrology, geochemistry and zircon geochronology in this study.

No.	Sample No.	Location	Latitude and longitude	Rock types
1	PG-1	Naruvamoodu	N8°28'32" E77°00'31.99"	Gabbro
2	PG-2	Mukkunimala	N8°27'49.29" E77°01'15.11"	Gabbro
3	PG-3	Puvadakonam	N8°27'16.80" E77°01'55.30"	Gabbro
4	PG-4	Killiyoor	N8°5'53.72" E77°12'47.03"	Gabbro
5	PG-5	Chullalam	N8°40'44.50" E76°58'20.62"	Gabbro
6	PG-6	Vattappara	N8°35'33" E76°57'1.67"	Gabbro
7	PG-7	Mottakuzhi	N8°34'15.58" E76°55'48.83"	Gabbro
8	PG-8	Chengottukonam	N8°35'5.11" E76°53'56"	Gabbro
9	PG-9	Melattumuzhi	N8°42'53.86" E76°55'25.26"	Gabbro
10	PG-10	Kattaikonam	N8°36'7.72" E76°53'44.84"	Gabbro
11	PG-11	Ayiruppara	N8°36'6.29" E76°53'36.54"	Gabbro
12	PG-12	Kilimanoor	N8°46'13.28" E76°52'59.62"	Gabbro
13	PG-13	Nagaroor	N8°44'8.85" E76°50'50.92"	Gabbro
14	PG-14	Ozhukupara	N8°46'42.92" E76°52'16.54"	Gabbro
15	PG-15	Kunnanpara	N8°24'49.75" E76°58'27.13"	Gabbro
16	PG-16	Ponmudi	N8°45'25.97" E77°7'5.53"	Gabbro
17	PG-17	Chemaruthmukku	N8°45'55.39" E77°52'24.31"	Gabbro
18	PG-18	Unnanpara	N8°46'2.71" E76°48'0.01"	Gabbro
19	PG-19	Aramthanam	N8°36'7.72" E76°53'44.84"	Gabbro
20	PG-20	Venjaramudu	N8°41'29.80" E76°54'55.51"	Gabbro

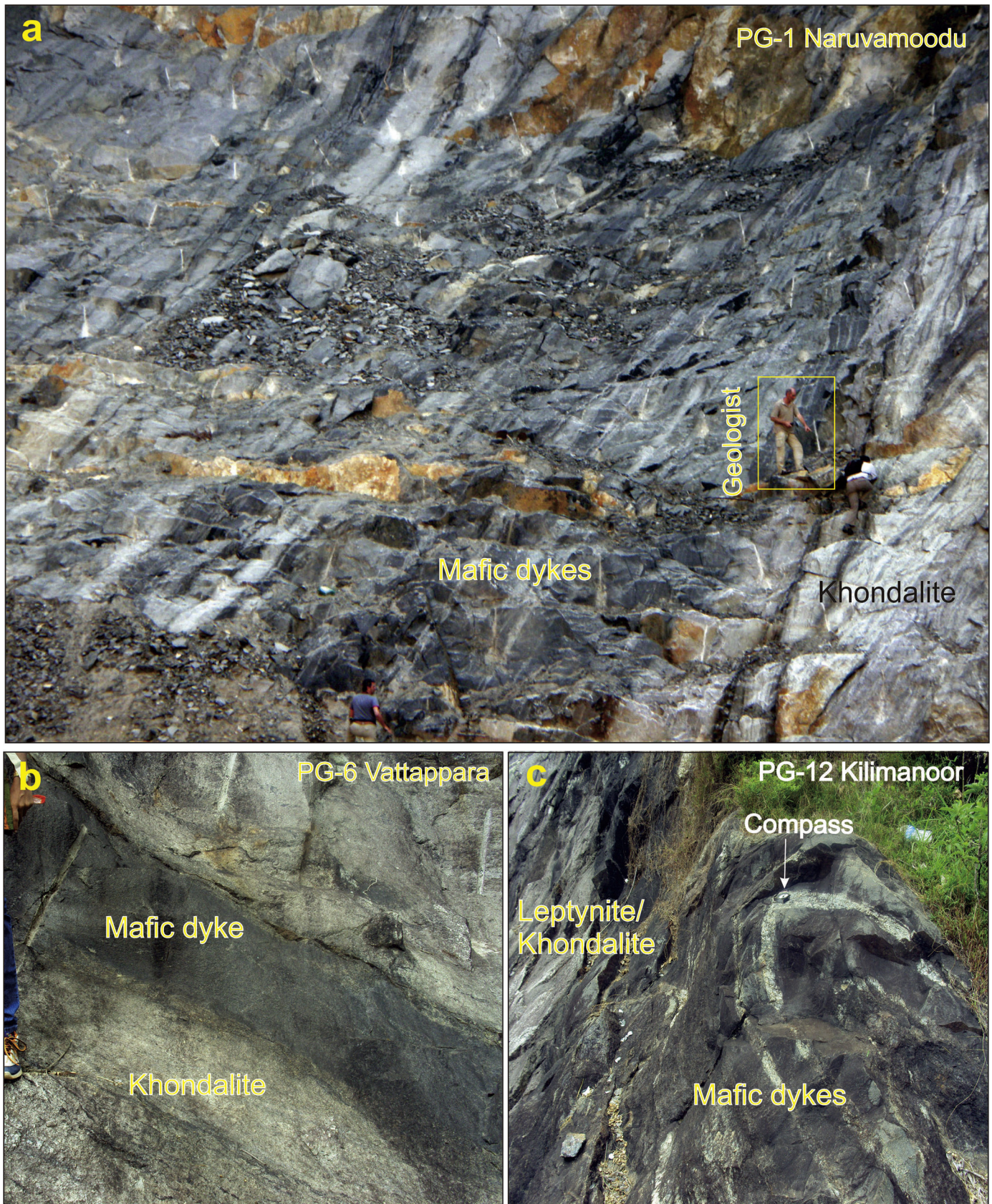


**Figure 3.** Representative field photographs of the gabbroic studies analyzed in this study. (a) Layer-parallel intrusions of mafic dykes emplaced within garnet-sillimanite-cordierite bearing metapelites (khondalites) at Naruvamoodu. (b) Mafic dyke showing sharp contact with host khondalite at Vattappara. (c) Set of folded mafic dykes emplaced within khondalite/leptynite units at Kilimanoor.

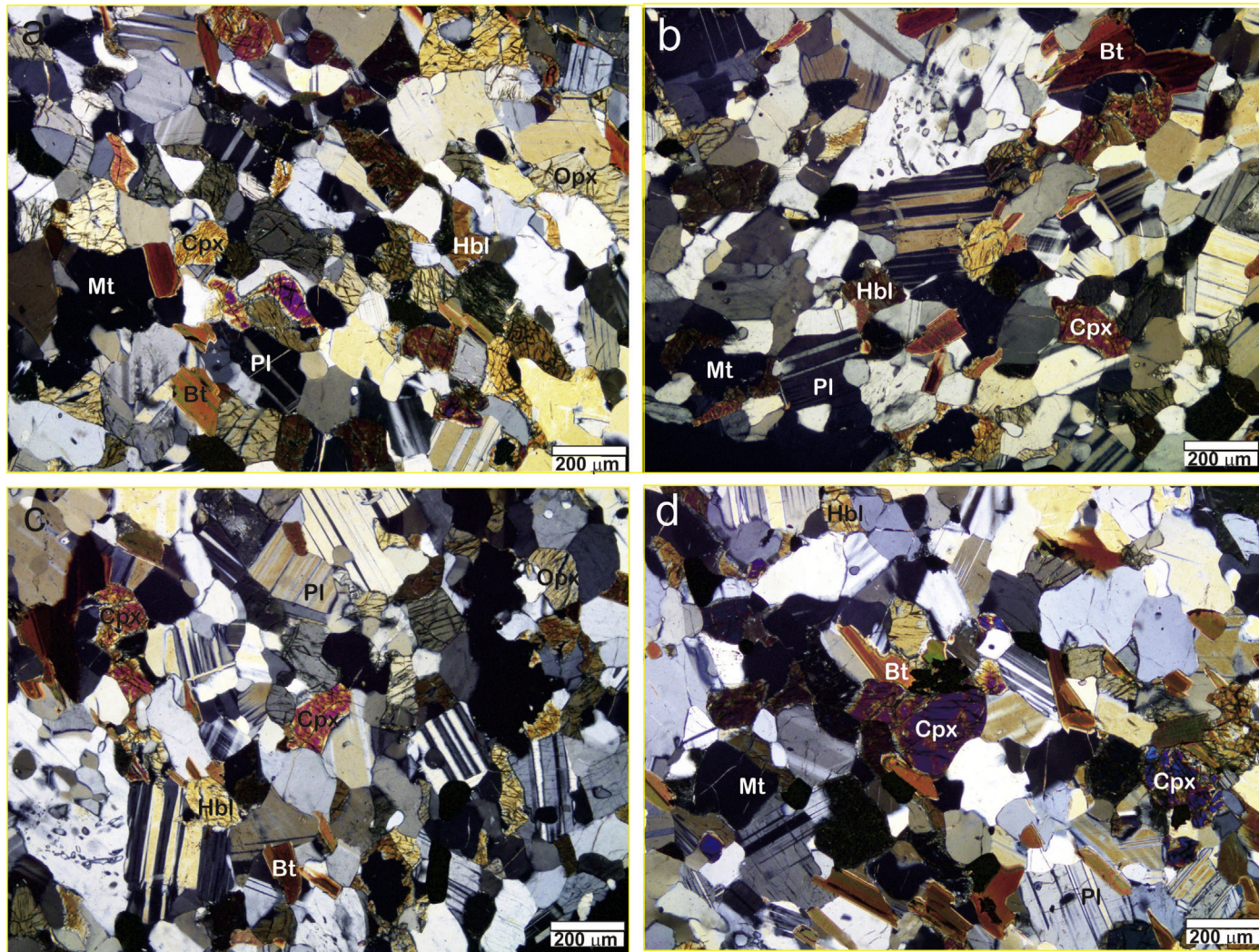


**Figure 4.** Representative photomicrographs showing the mineral assemblages in the gabbroic rocks of present study. Cpx: clinopyroxene, Opx: orthopyroxene, Pl: plagioclase, Hbl: hornblende, Bt: biotite, Mt: magnetite. All photos in crossed nicols.

kupara, Kunnanpara, Chemaruthmukku and Aramthanam areas of the Trivandrum block are presented in [Supplementary Table 1](#). The studied samples are characterized by a restricted range of SiO<sub>2</sub> contents (45.1–50.3 wt.%), moderate to high TiO<sub>2</sub> (0.98–4.81 wt.%), moderate concentrations of MgO (5.05–7.13 wt.%) and CaO (8.61–12.6 wt.%), with elevated abundance of Al<sub>2</sub>O<sub>3</sub> (11.9–16.32 wt.%) and Fe<sub>2</sub>O<sub>3</sub> (14.83–20.4 wt.%). The Mg# values and total alkali content for the samples range from 19 to 29 and 0.9 to 3.85 respectively. The studied samples plot in the field of gabbro in the total alkali vs. silica (TAS) diagram ([Fig. 5](#); after Cox et al., 1979 and adapted from Wilson, 1989). Thus, these dykes/sills are classified as dominantly gabbros and they are chemically analogous to high Fe tholeiitic basalts as reflected from their plots on Jensen's diagram ([Fig. 6a](#)). This observation is in accordance with the distinct tholeiitic nature of the studied samples on AFM ternary plot ([Fig. 6b](#)) of Irvine and Baragar (1971). The gabbros clearly correspond to the tholeiite series on FeO<sup>T</sup> vs. FeO<sup>T</sup>/MgO plot ([Fig. 6c](#)) and low K-tholeiite to medium-K calc-alkaline series in the K<sub>2</sub>O-SiO<sub>2</sub> diagram ([Fig. 6d](#)).

## 5.2. Trace and rare earth elements

The transitional compatible trace element chemistry for the studied samples is marked by depleted Ni (17.24–59.97 ppm), Cr (23.73–101.03 ppm) and Co (50.57–85.74 ppm) concentrations. The large ion lithophile elements (LILE) viz. Rb, Sr and Ba show variable compositions in the range of 0.9–21.61 ppm, 14.12–165.2 ppm and 6.92–236.63 ppm respectively. Among the high field strength elements (HFSE), Nb (3.4–30.2 ppm), Zr (13–441 ppm) and Y (17.5–69.3 ppm) display moderate to elevated abundance, whereas Hf, Ta, and Th record relatively lower concentrations ([Supplementary Table 1](#)). These rocks show variable total REE contents ranging from 32.8 ppm to 164.4 ppm. Chondrite normalized REE patterns ([Fig. 7a,c,e](#)) of the gabbros show slight to moderate enrichment in LREE and flat to fractionated HREE patterns with negligible to negative Eu anomalies and mild positive anomalies of Ce. The (La/Sm)<sub>N</sub> = 0.5–2.43, (Sm/Yb)<sub>N</sub> = 0.96–2.53, (Gd/Yb)<sub>N</sub> = 1.03–2.3 and (La/Yb)<sub>N</sub> = 0.65–3.6 collectively suggest feeble to pronounced LREE/MREE and LREE/HREE fractionation

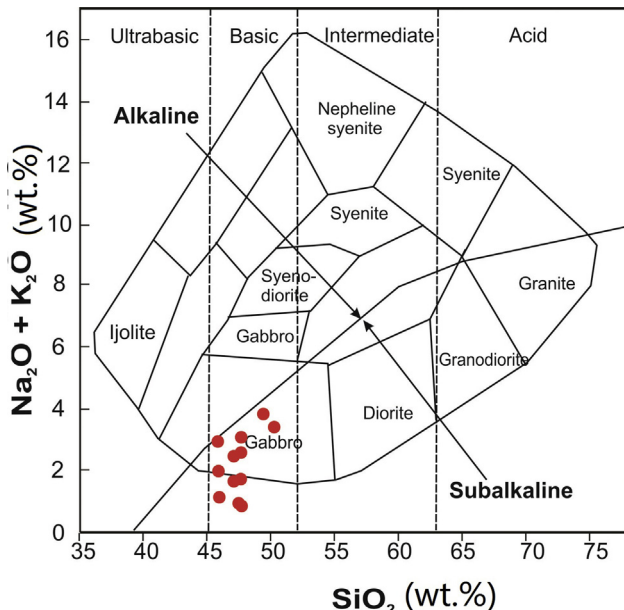


**Figure 5.** Total alkali vs. silica diagram in which the studied rocks plot in the field of gabbro (after Cox et al., 1979, and adapted from Wilson, 1989).

patterns with moderate to prominent MREE/HREE fractionation. Primitive mantle-normalized trace element abundance patterns (Fig. 7b,d,f) show distinct negative anomalies for Th, Zr–Hf and Ti conforming to relative HFSE depletion with LILE and LREE enrichment. The multi-element patterns for these rocks are marked by pronounced positive anomalies at Nb and Ta indicating enrichment of these elements over LILE and LREE.

## 6. Zircon U–Pb geochronology and trace elements

### 6.1. Zircon U–Pb geochronology

Representative cathodoluminescence (CL) images of the zircon grains from the three gabbro samples of PG-6, PG-15 and PG-17 analyzed in this study are shown in Figs. 8–10, respectively. The U–Pb analytical data are given in Supplementary Table 2, and plotted in concordia diagrams together with age data histograms and probability curves in Figs. 11–13. A brief description of the zircon characteristics and age results from individual samples is given as below. For different samples with or without different age groups, the weighted mean age is presented with two types of uncertainty: analytical uncertainty and total uncertainty. For example,  $^{206}\text{Pb}/^{238}\text{U}$  weighted mean age of  $507.3 \pm 3.6$  [10.8] Ma (MSWD = 1.13,  $N = 27$ ) indicates that 3.6 Ma is the analytical uncertainty, and the 10.8 Ma is the total uncertainty (SQRT: analytical uncertainty<sup>2</sup> + systematic uncertainties<sup>2</sup>; see Spencer et al., 2016, 2017).

Zircon grains from sample PG-6 are colorless or slightly brownish. They are prismatic and stumpy with size mostly larger than  $80 \mu\text{m} \times 100 \mu\text{m}$  and aspect ratios higher than 1:1. In CL images, all the zircons display striped zoning and show clearly magmatic origin (Fig. 8). Zircon grains from sample PG-15 are also colorless and range from  $60 \mu\text{m} \times 80 \mu\text{m}$  to  $100 \mu\text{m} \times 200 \mu\text{m}$  in size with aspect ratios of 3:1 to 1.5:1. In CL images, they show weakly patch zoning or striped zoning (Fig. 9). Some grains are mostly homogeneous without any clear zoning. The zircon grains in sample PG-17 are larger in size than those in samples PG-6 and PG-15. They show  $100 \mu\text{m} \times 200 \mu\text{m}$  size with aspect ratios higher than 2:1. In CL images, all the zircon grains display weakly oscillatory zoning or striped zoning (Fig. 10) suggesting magmatic origin.

Thirty-five zircon spots were analyzed in sample PG-6 and the results show low contents of Pb (17.37–32.79 ppm with one exception of 165.04 ppm) and U (43.79–97.72 ppm), with relatively lower Th contents (8.07–17.28 ppm, only one exception of 36.46 ppm) (Supplementary Table 2). Among the 35 zircon spots, 34 analysis including 27 concordant ones and 7 discordant ones show  $^{206}\text{Pb}/^{238}\text{U}$  spot ages in the range of  $483 \pm 18$  Ma to  $554 \pm 20$  Ma. The concordant plots yield a  $^{206}\text{Pb}/^{238}\text{U}$  mean age of  $507.3 \pm 3.6$  [10.8] Ma (MSWD = 1.13,  $N = 27$ ) (see Fig. 11a–c) which is considered as the crystallization age of this rock. In this zircon group, one analysis from the discordant spots shows an older  $^{206}\text{Pb}/^{238}\text{U}$  age of  $554 \pm 20$  Ma which may suggest the crystallization age of the inherited zircons. The other zircon grain displaying the highest Pb content and lowest U and Th contents in the analyzed zircons from this sample is discarded in the concordia plots due to the large error.

Thirty-five zircon grains were analyzed from the gabbro sample PG-15. The results show very low Pb and U and contents, however they display slightly larger ranges than those of zircons in sample PG-6 (Supplementary Table 2). The dominant zircon plots are concordant and divided into three groups. One group includes seven zircon grains which are rounded in shape. Among these, five are concordant spots and the other two are discordant ones. The seven zircons display  $^{206}\text{Pb}/^{238}\text{U}$  spot ages ranging from  $561 \pm 19$  Ma to  $581 \pm 20$  Ma and yield an older  $^{206}\text{Pb}/^{238}\text{U}$  mean age of  $572.9 \pm 8.6$  [14.3] Ma (MSWD = 0.63,  $N = 5$ ) (see Fig. 12a–d). The main zircon group with 19 concordant analysis and 8 discordant ones are the grains with prismatic feature and showing  $^{206}\text{Pb}/^{238}\text{U}$  spot ages of  $492 \pm 16$  Ma to  $539 \pm 18$  Ma. In this group, the concordant spots yield a younger  $^{206}\text{Pb}/^{238}\text{U}$  mean age of  $505.1 \pm 3.9$  [10.8] Ma (MSWD = 0.54,  $N = 19$ ) (see Fig. 12a,b,e,f). The remaining one zircon spot is discordant suggesting lead-loss and shows  $^{206}\text{Pb}/^{238}\text{U}$  age of  $630 \pm 21$  Ma indicating inherited zircon in the basement rocks. The  $^{206}\text{Pb}/^{238}\text{U}$  mean age of ca. 573 Ma is also considered as the age of the inherited zircons probably caught up from the basement rocks. The  $^{206}\text{Pb}/^{238}\text{U}$  mean age of ca. 505 Ma is taken to present the crystallization age of this rock.

Twenty-six zircon grains were analyzed from the gabbro sample PG-17. The U–Pb data show very low contents of Pb (1.85–4.87 ppm), U (5.50–14.42 ppm) and Th (0.33–1.61 ppm) (Supplementary Table 2). All the plots are concordant and display  $^{206}\text{Pb}/^{238}\text{U}$  mean age of  $494.3 \pm 3.8$  [10.6] Ma (MSWD = 0.36,  $N = 26$ ) (see Fig. 13a–c). The single age population in this rock corresponds to its crystallization age.

### 6.2. Zircon trace elements

Trace element analysis was performed on the magmatic zircon domains of the three samples which were dated using U–Pb geochronology by LA-ICPMS. The chondrite-normalized REE diagrams (normalizing values are after Sun and McDonough, 1989) are presented in Fig. 14. The analytical data are presented in Supplementary Table 2.

Most of the zircons from the gabbros are enriched in heavy REE compared to light REE, and show a distinct positive Ce anomaly as well as negative Eu anomaly. The contents of REE range from 121 ppm to 315 ppm for sample PG-6, 139 to 335 ppm for sample PG-15 and 136 ppm to 321 ppm for sample PG-17 with two analysis in this sample showing higher REE contents of 487 ppm and 665 ppm, respectively.

Thirty-three analyses from gabbro sample PG-6 preserve highly fractionated chondrite-normalized LREE and HREE profiles ( $(\text{La}/\text{Sm})_{\text{N}} = 0.005$ –0.016) with moderate europium anomalies ( $(\text{Eu}/\text{Eu}^*) = 0.136$ –0.368) and moderately fractionated chondrite-normalized HREE patterns ( $\text{Yb}_{\text{N}} = 237$ –648). Twenty-five analyses from gabbro sample PG-16 show the same features of REE patterns

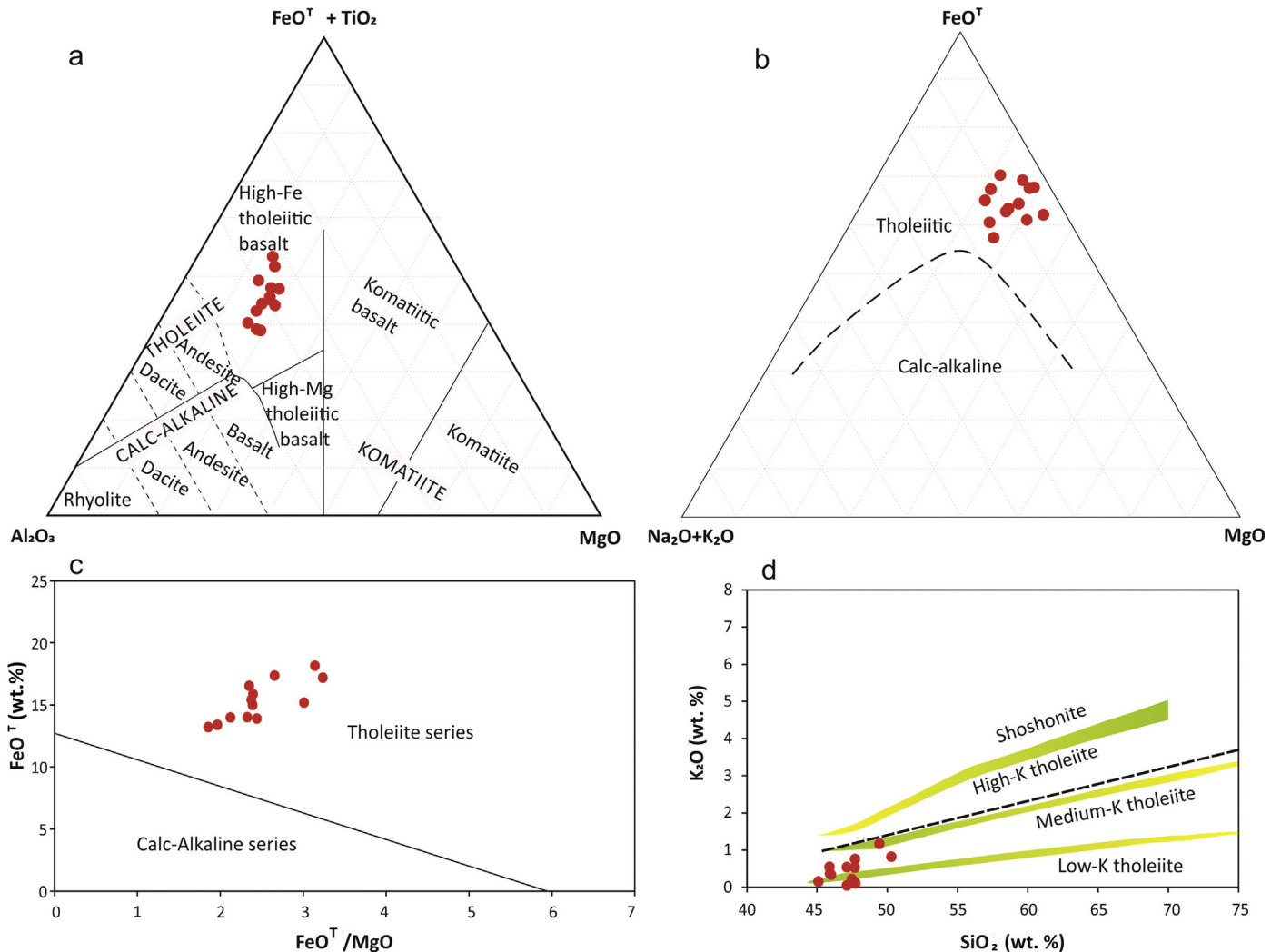


**Figure 6.** (a) Plots of studied samples reflecting High Fe tholeiitic character in  $\text{TiO}_2\text{--Al}_2\text{O}_3\text{--MgO}$  diagram (after Jensen, 1976). (b)  $(\text{Na}_2\text{O} + \text{K}_2\text{O})\text{--FeOT}\text{--MgO}$  (AFM) diagram (after Irvine and Baragar, 1971) showing the tholeiitic trend for the studied dykes. The dividing line is after Irvine and Baragar (1971). (c)  $\text{FeOT}$  vs.  $\text{FeOT}/\text{MgO}$  plot for the studied rocks reflecting their tholeiitic composition. (d)  $\text{SiO}_2$  vs.  $\text{K}_2\text{O}$  diagram showing the plots of gabbros corresponding to low K tholeiite to medium K calc alkaline series. The compositional fields are after Rollinson (1993).

with highly fractionated chondrite-normalized LREE and HREE profiles ( $(\text{La/Sm})_{\text{N}} = 0.001\text{--}0.019$ ), moderate-highly europium anomalies ( $(\text{Eu/Eu}^*) = 0.085\text{--}0.349$ ) and moderately fractionated chondrite-normalized HREE patterns ( $\text{Yb}_{\text{N}} = 259\text{--}635$ ). Twenty-six analyses from gabbro sample PG-17 also yield the same features of REE patterns as those in gabbro samples PG-6 and PG-15. The data display highly fractionated chondrite-normalized LREE and HREE profiles ( $(\text{La/Sm})_{\text{N}} = 0.005\text{--}0.023$ ) and moderate europium anomalies ( $(\text{Eu/Eu}^*) = 0.254\text{--}0.563$ ) with moderately fractionated chondrite-normalized HREE patterns ( $\text{Yb}_{\text{N}} = 291\text{--}1261$ ).

The uniformity in REE patterns may represent the same source materials for the gabbros in this study.

## 7. Discussion

### 7.1. Tectonic implications

The gabbro dykes and sills show intrusive relations act with the host metapelites and the field settings suggest emplacement after the peak metamorphism of the surrounding basement rocks.

However, lack of chilled margins, minor gradational contacts in some cases, and the co-folded nature suggest that both the dykes/sills and the host rocks were subjected to common late stage tectonics. The dominant clinopyroxene-plagioclase assemblage in these rocks is typical of gabbroic suites with the marginal portions showing orthopyroxene, garnet and quartz suggesting interaction with the aluminous host rocks. Geochemically, the rocks are characterized by enrichment of LILE (e.g. Rb, Sr, Ba), LREE and depletion of HFSE (e.g. Zr, Hf) relative to typical primitive mantle values with negative anomalies at Zr-Hf and Ti on primitive mantle normalized multi-element spider diagram (Fig. 7). These geochemical signatures including high LILE/HFSE and low HFSE/LILE ratios are characteristically attributed to a subduction zone magmatic regime associated with typical island arc environment (Sheraton et al., 1990; Zhao et al., 1995; Yang et al., 2016a,b). On  $\text{TiO}_2\text{--MnO}\text{--P}_2\text{O}_5$  triangular diagram, the studied samples plot in the field of island arc tholeiite (IAT) corroborating an arc-tholeiite environment for the generation of parent magmas (Fig. 15). The arc affinity of these rocks is further reflected on the  $\text{FeO}^*/\text{MgO}$  vs.  $\text{TiO}_2$  plot (Fig. 16a) where the samples cluster in the arc front domain. However, primitive mantle-normalized trace element abundance patterns

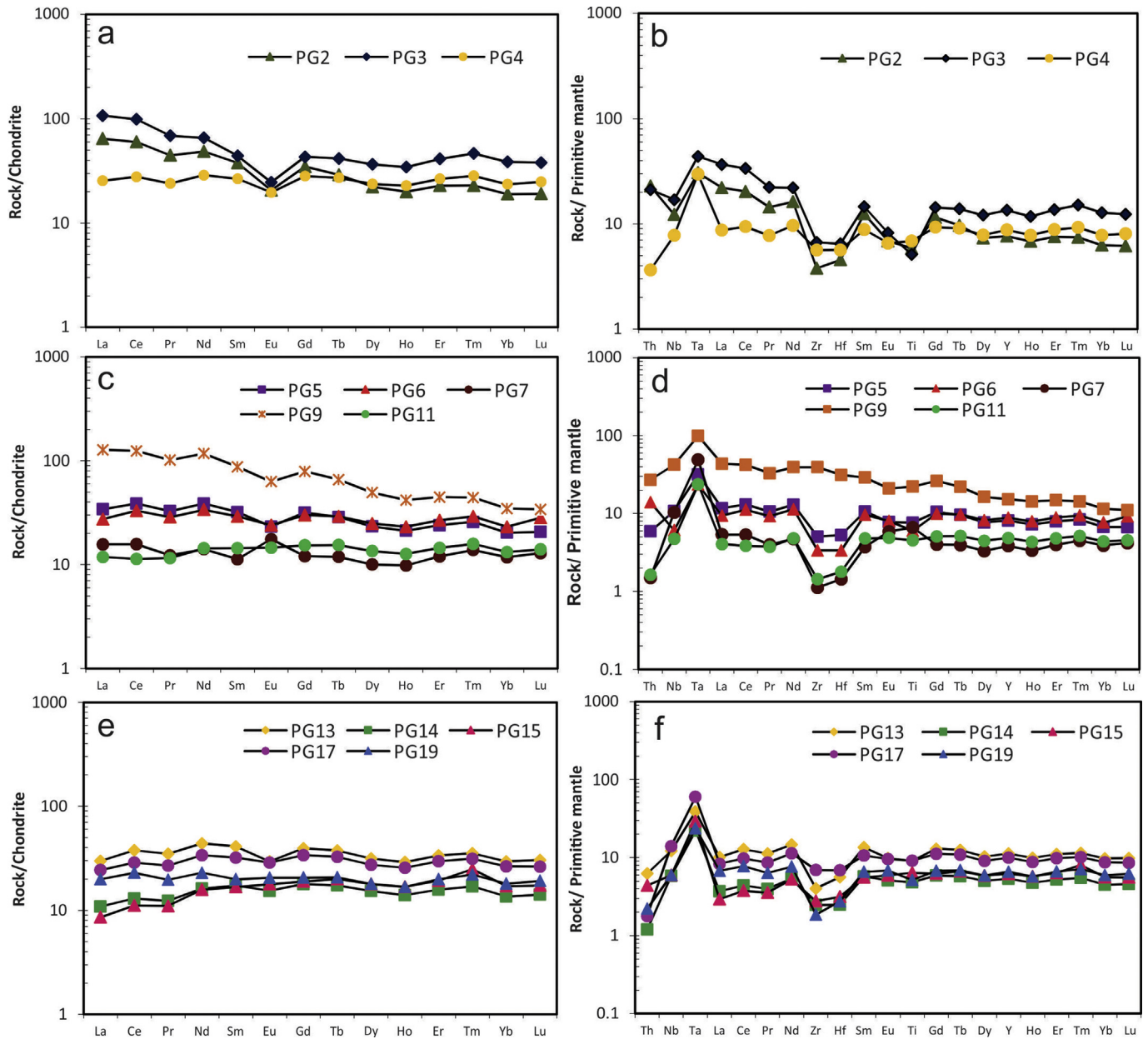


**Figure 7.** Chondrite normalized REE patterns and Primitive mantle-normalized multi-element plots for the studied dykes. Normalizing factors are from Sun and McDonough (1989).

showing positive anomalies at Nb and Ta warrants speculation on involvement of an asthenospheric mantle component containing recycled oceanic slab components from ancient subduction processes. On  $TiO_2$  vs.  $Al_2O_3$  binary diagram (Fig. 16b), the studied samples straddle the fields for within plate and arc related setting thereby reflecting a geodynamic transition from arc to intraplate affinity and substantiating ocean closure to collisional tectonics at active continental margins (Santosh, 2010, 2013; Polat, 2012; Ray et al., 2013; Santosh et al., 2015, 2017). The geochemical signatures of the gabbros are in compliance with the generation of parent melts from heterogeneous source region and their emplacement in a transitional tectonic environment extending from subduction to post-collisional intraplate conditions. The elevated Nb abundances and distinct Nb-Ta positive anomalies for these rocks invoke involvement of an upwelling asthenospheric component carrying recycled, residual, oceanic crust of Precambrian subduction events (Hofmann, 1997; Safonova et al., 2008;

Cabral et al., 2013). Therefore, the tectonic discrimination parameters together with distinct trace element signatures point toward contribution from the subduction-accretion-collision processes for the origin and emplacement the gabbro dykes. Continental collisions at the waning stages of subduction process lead to steepening and tearing of the subducted slab followed by break-off. This progressive disruption of the subducted slab provides a window to the hot, sub-slab asthenospheric mantle to migrate and rise through this gap (Keskin, 2003, 2007; Ferrari, 2004). The upwelling and inflow of asthenospheric mantle at shallow depth through a slab window results in adiabatic decompression melting. Mixing between two distinct mantle domains including the subduction-modified, metasomatized mantle wedge and the upwelled asthenospheric melts through slab break-off generates magmas that accumulate and pond at the base of sub-continental lithospheric mantle (SCLM) and fractionates in a sub-surface magma chamber in a post-collisional, intraplate tectonic regime. Post-

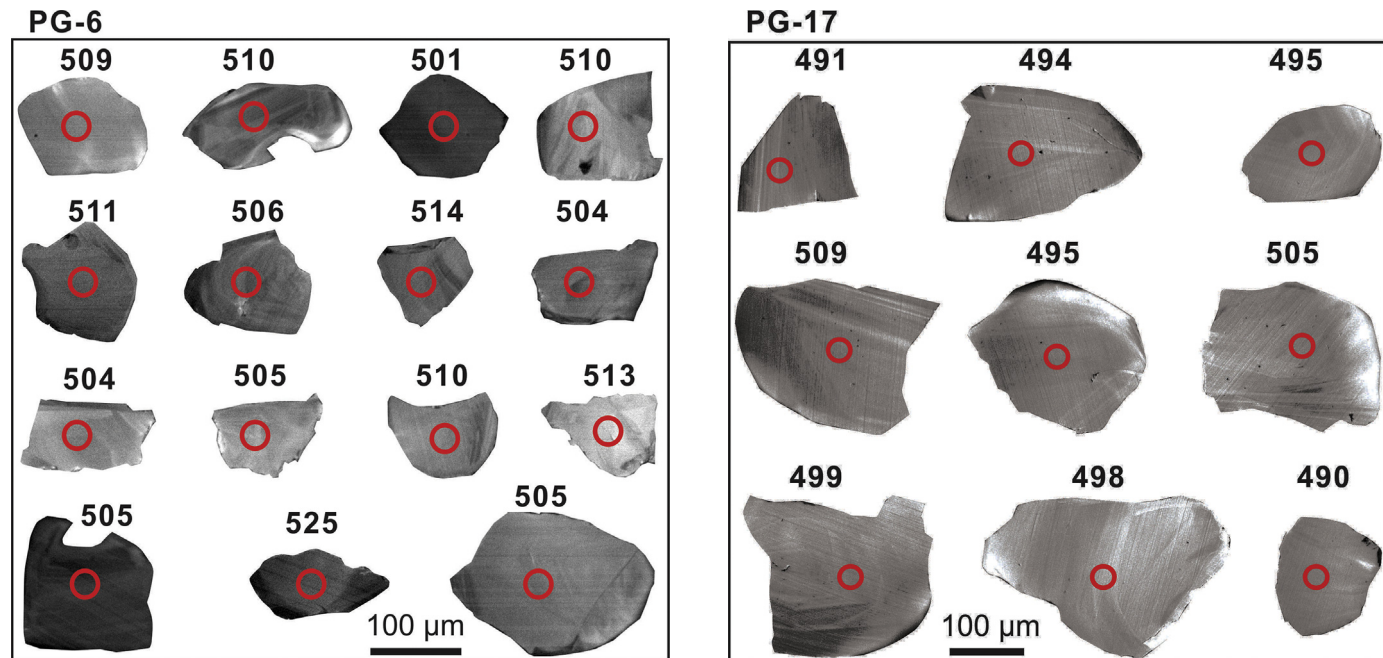


**Figure 8.** CL images of zircon grains in sample PG-6 showing age values in Ma and analyzed spots.

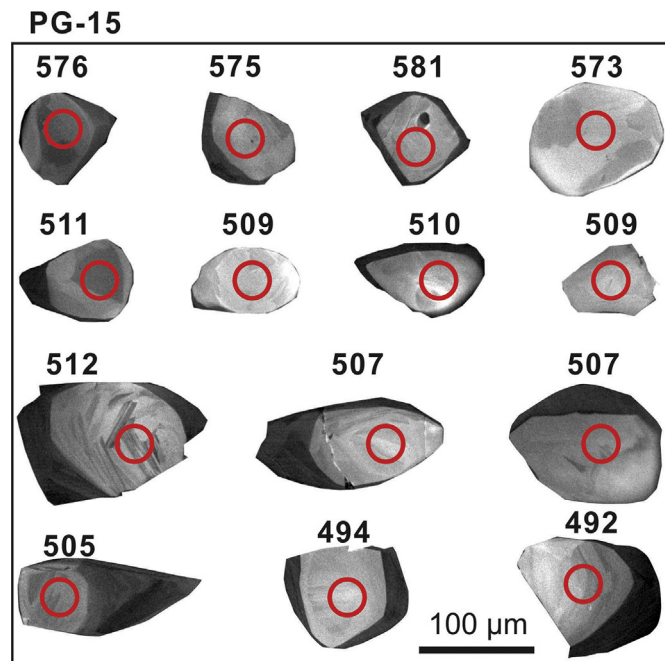


**Figure 9.** CL images of zircon grains sample PG-15 showing age values in Ma and analyzed spots.

collisional extension, lithospheric fracturing and rifting permit the evolved melts to migrate upward to shallower crustal domains. These mechanisms provide the most viable explanation to account for the distinct geochemical and tectonic affiliations for the studied rocks. The gabbroic rocks do not resemble typical intracontinental plume-generated or typical island arc related magmatism, and we infer that these rocks were emplaced as post-collisional intrusions in an extensional setting associated with termination of convergence and slab-break-off. The magma parental to these rocks was derived through (1) partial melting of subduction-related,

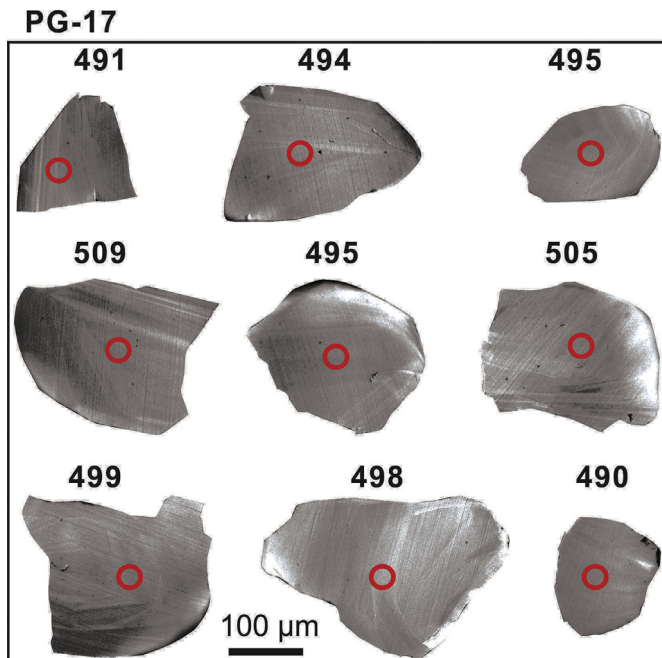


**Figure 10.** CL images of zircon grains sample PG-17 showing age values in Ma and analyzed spots.

metasomatized mantle wedge in a continental arc setting; (2) interaction with upwelling asthenospheric melts following slab break-off. The high Nb contents and positive Nb–Ta anomalies of the studied rocks are attributed to inflow of asthenospheric melts containing ancient recycled subducted slab components and/or fusion of subducted slab materials owing to upwelling of hot asthenosphere through slab break-off. The accumulation of parent melts beneath SCLM and sub-surface magma chamber processes triggered reworking of older crustal components.

## 7.2. Crustal contamination and crystallization history

The ascent of mantle-derived magmas through the continental lithosphere to the surface makes crustal contamination inevitable, either through assimilation-fractional crystallization (AFC) or thermal erosion of floor rocks, due to their higher liquidus temperature (Hawkesworth et al., 1984; Mahoney, 1988; Carlson, 1991; Hergt et al., 1991; Gallagher and Hawkesworth, 1992; Saunders et al., 1992; Sweeney et al., 1994; Song et al., 2001, 2008). Trace element compositions provide appropriate geochemical tracers to decipher the open and closed system magmatic processes like crustal assimilation and fractional crystallization (Lassiter et al., 1995; Condie, 2003; Reichow et al., 2005; Shellnutt et al., 2014). The studied samples have  $K_2O/P_2O_5$  ratios ranging from 0.4 to 11.7 suggesting variable input from silicic crustal components from older sialic basement or wall rock (of granitic composition) and assimilation during ascent of parent melts. The  $TiO_2/P_2O_5$  ratios (4.4–14.3) also suggest that the parental melts were affected by contamination from granitic continental crust (Carlson and Hart, 1988). Thompson et al. (1984) considered the La/Nb ratio as a suitable index of crustal contamination in magmas and suggested that OIB, continental alkali basalts and kimberlites have  $La/Nb < 1$ , whereas that of CFB magmas ranges from 0.5 to 7. The La/Nb ratios (0.5–2.1) of the studied samples are in accordance with variable degrees of crustal contamination of parent magma in an intraplate setting marked by extensional tectonics (Peate et al., 1999; Song et al., 2001). The Nb/Th ratio in Archean basalts is considered as a

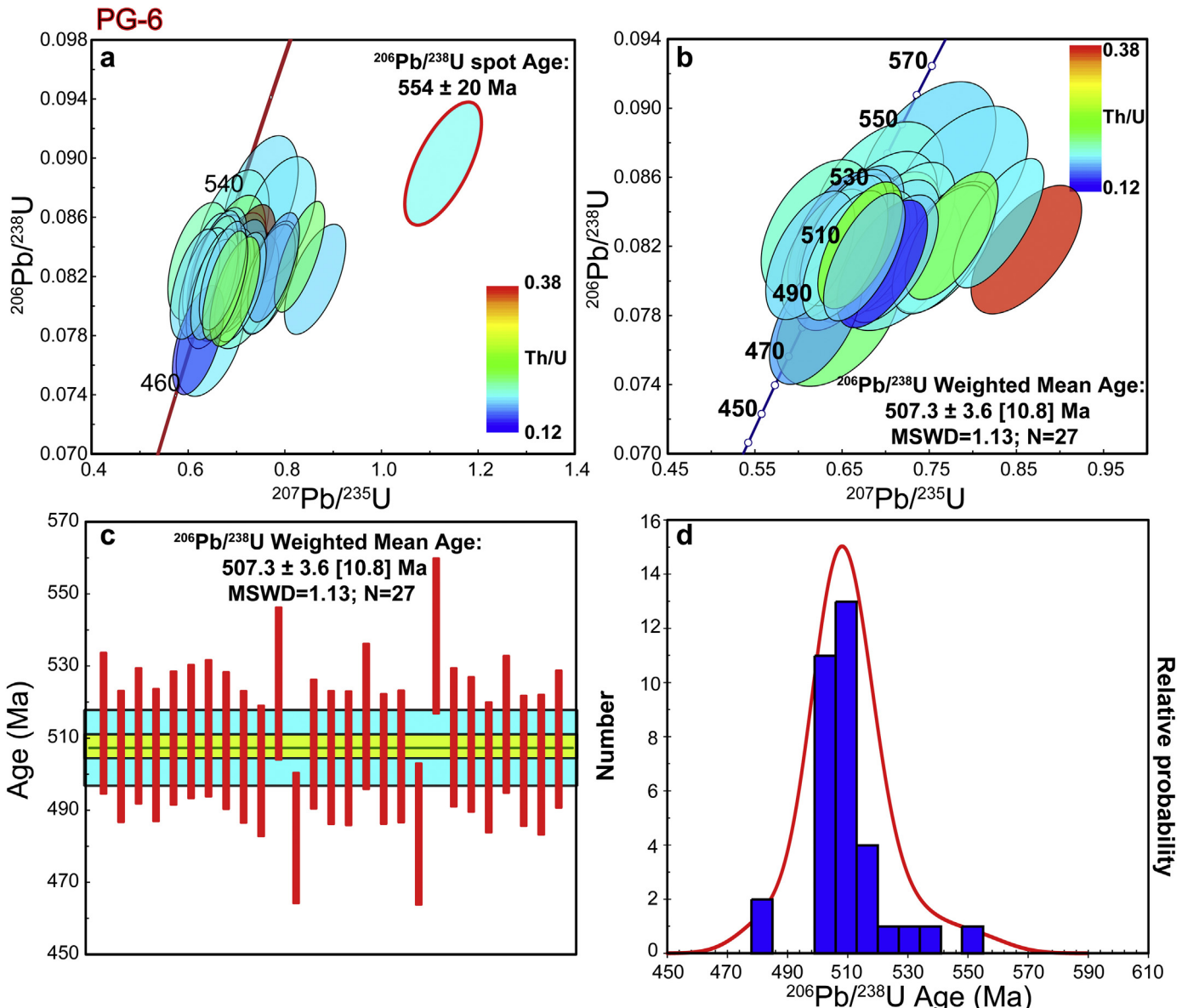


**Figure 11.** Concordia plots, age data bar charts and histograms of zircon grains in sample PG-6.

monitor of the extent and timing of extraction of continental crust from the mantle (Sylvester et al., 1997). The Nb/Th ratio of primitive mantle is 8, whereas in continental crust it is  $\sim 1.1$  (Taylor and McLennan, 1985; Sun and McDonough, 1989; Rudnick and Gao, 2003). This geochemical feature suggests Nb depletion with distinct enrichment in Th within crust attesting to subduction-related magmatism and associated accretionary processes at an active continental margin considered to be a principal mechanism for Precambrian crustal growth (Polat, 2012; Santosh, 2013; Santosh et al., 2013, 2017). Besides considering contamination by continental crust as one of the factors, the wide variation in Nb/Th ratios for the studied samples (3.7–66.15) in conjunction with enhanced Nb contents and positive Nb-Ta anomalies suggest at least three conditions that possibly influenced the genesis of precursor magma for these rocks from a heterogeneous sub-arc mantle source. These are: (1) recycled, residual slab components (RSC) of Precambrian subduction events entrained by upwelling asthenospheric mantle through slab window; (2) subducted oceanic slab

melts metasomatizing the mantle wedge peridotite during slab-break-off; (3) melting of Nb-bearing metasomatic phases like amphibole in the mantle wedge (Sajona et al., 1996; Keskin, 2003; Liao et al., 2018; Saha et al., 2017).

The overall major oxide compositions of the gabbros suggest that the evolution of parental melts was dominantly controlled by fractional crystallization process. The studied samples have low Mg# (19–29) endorsing an evolved chemistry marked by extensive fractional crystallization of magma either in magma chamber or during ascent. Ni and Cr concentrations of the studied rocks are lower than that of primary mantle melts (Ni > 200 ppm, Cr > 400 ppm) of an olivine dominated source, thereby implying widespread fractional crystallization processes and pronounced magmatic evolution. Lower concentrations of compatible transition metals support the contention that these rocks are not derived from primary magmas and have experienced considerable fractional crystallization prior to eruption. Low Mg# for the studied samples attests to their derivation from a mantle more Fe-rich than normal

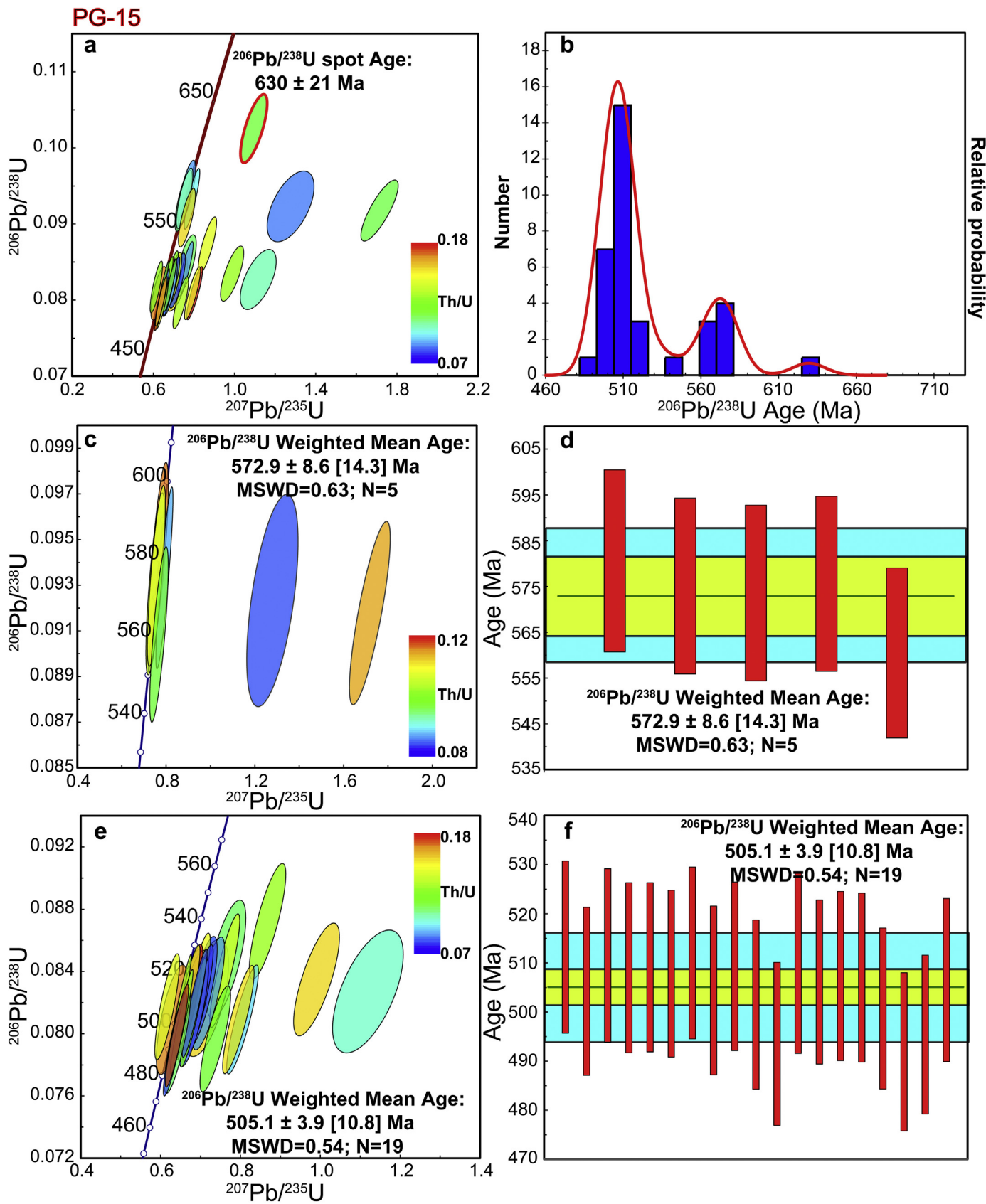
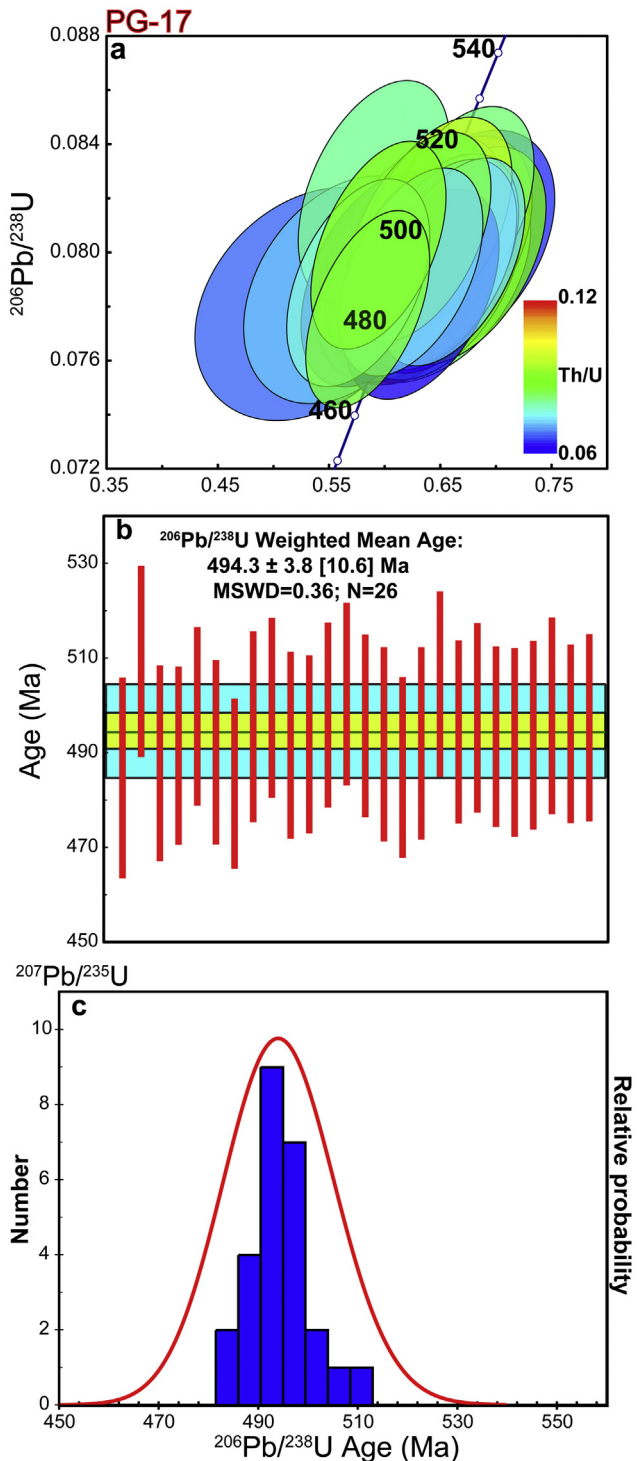
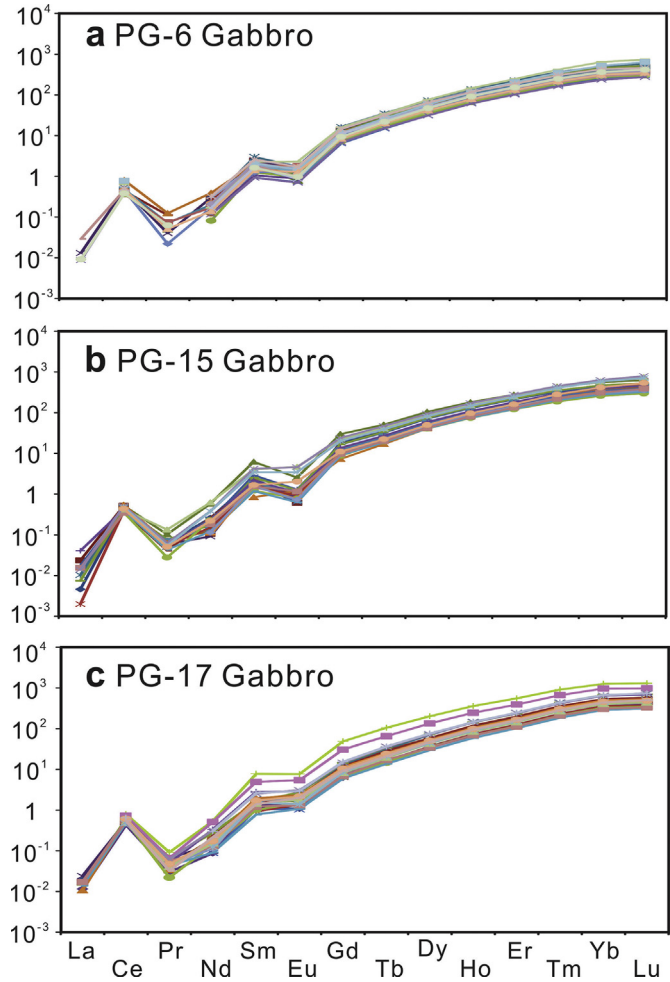


Figure 12. Concordia plots, age data bar charts and histograms of zircon grains in sample PG-15.



**Figure 13.** Concordia plots, age data bar charts and histograms of zircon grains in sample PG-17.

MORB-OIB compositions. The evolved nature of these and relatively high Zr contents are equated with magmatic differentiation controlled by extensive fractional crystallization over a wide range of pressure. The major and trace element variation patterns and relatively higher total alkali contents (0.9–3.85) of the gabbros point toward fractional crystallization and crustal assimilation of the parent magma.



**Figure 14.** Chondrite normalized REE patterns for the zircons from gabbros in Tri-vandrum Block. Normalizing factors are from Sun and McDonough (1989).

### 7.3. Mantle processes: role of asthenosphere and subduction components

The tectonic affiliations of the gabbros coupled with their distinct geochemical features endorse a heterogeneous mantle source with collective melt contributions from sub-slab asthenospheric mantle upwelling through slab break-off and arc-related metasomatized mantle wedge in a subduction-collision regime at active continental margin. In oceanic and continental convergent margin systems, the two principle contributors to arc magmatism are the metasomatized peridotite in the mantle wedge and the subducting oceanic lithosphere (McCulloch and Gamble, 1991; McCulloch, 1993; Yogodzinski et al., 1995; Saccani et al., 2004, 2011; Tatsumi, 2005; Kimura and Yoshida, 2006; Dilek et al., 2008; Sato et al., 2013; Shuto et al., 2013; Iwamori and Nakamura, 2015; Santosh et al., 2015). Magma compositions in island arcs are influenced by the tectonic framework along the arc, geometry of the subducting plate, modification and enrichment of depleted mantle wedge by influx of materials released from subducting oceanic slab (slab-dehydrated fluids, silicate slab melts and subducted sediments) and melting conditions in the mantle wedge (Woodhead et al., 1993, 2001; Ewart et al., 1998; Bourdon et al., 2002; Foley et al., 2002; Schuth et al., 2009). The entire episode of subduction, from its initiation to termination, is marked by a gradual progress from early decompression melting of a depleted lherzolitic mantle to fluid-fluxed hydrous melting of fertile

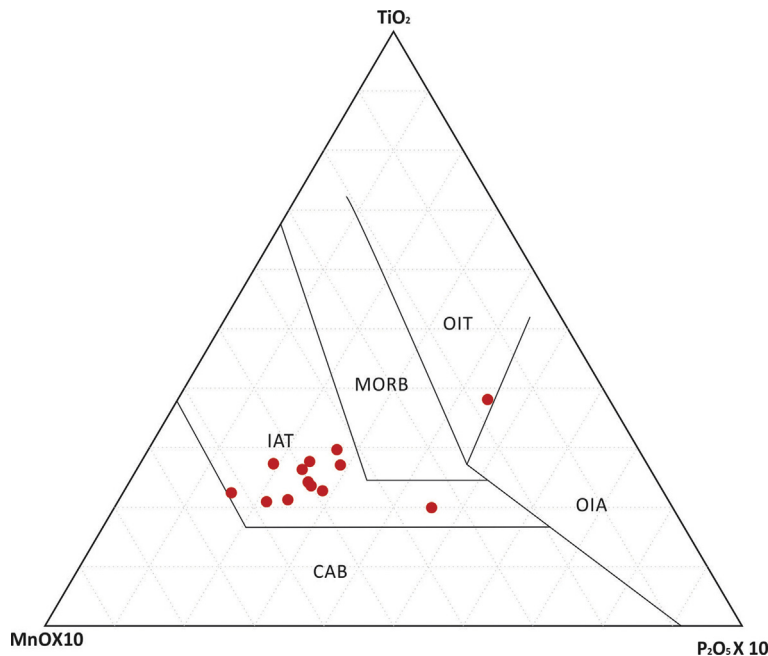


**Figure 15.**  $\text{MnO}-\text{TiO}_2-\text{P}_2\text{O}_5$  triangular diagram (after Mullen, 1983) classifying the studied rocks as island arc tholeiites (IAT).

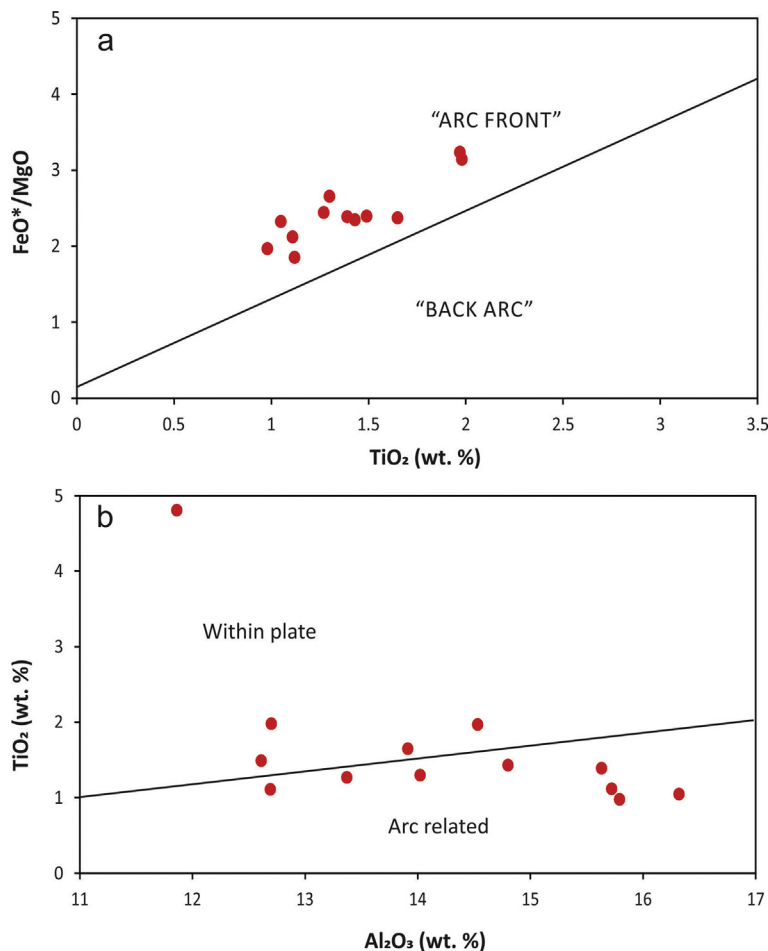


**Figure 16.** (a) Plots of the studied rocks in the “arc front” field of  $\text{FeO}^*/\text{MgO}$  vs.  $\text{TiO}_2$  diagram indicating their tectonic affinity to convergent plate margin setting. (b)  $\text{TiO}_2$  vs.  $\text{Al}_2\text{O}_3$  diagram (after Muller et al., 1992) showing the plots of gabbros straddling the fields for within plate and arc related setting.

harzburgitic mantle that has been significantly modified by subduction derived fluids/sediments, to melting of subducted slab. Basaltic magmas of tholeiitic to calc-alkaline compositions are generated by partial melting of mantle wedge metasomatized by relative contributions from various subduction-derived components including slab-dehydrated fluids and subducted sediments during juvenile and matured stages of subduction (Elliott et al., 1997; Elburg et al., 2002; Ganguly et al., 2016).

The trace elemental budget of magmatic rocks generated at subduction zones reflect contribution of mantle wedge and slab derived components (Defant and Drummond, 1990; McCulloch and Gamble, 1991; Plank and Ludden, 1992; Konig et al., 2010). The slightly depleted to elevated abundances of LREE and LILE relative to depletion of HREE and some HFSE in the studied rocks account for selective transport of elements from slab to wedge. The fluid mobile large ion lithophile element (LILE) having low ionic potential were released with the fluids dehydrated from the subducted oceanic slab and entered the mantle wedge resulting into fluid-driven metasomatism and partial melting. However, the high field strength elements (HFSE) due to their fluid immobile nature were retained in the dehydrated slab in a subduction regime (Stern et al., 1991; Pearce et al., 1992; Plank and Langmuir, 1993, 1998; Konig et al., 2010). The migration of slab-dehydrated fluids promotes mobilization of elements and contributes to 3%–25% of melting of mantle wedge at a depth of 30–50 km and at 1250–1350 °C mantle temperatures (Plank et al., 2013; Kimura and Nakajima, 2014). Therefore, fluid transportation from slab to mantle wedge and its role in subduction zone magmatism supports the contention that island arc tholeiites contain 1–8 wt.% of subduction derived hydrous fluids compared to the mid oceanic ridge basalts (MORB, 0.2 wt.%) and ocean island basalts (OIB, 0.8 wt.%; Saal et al., 2002; Fei et al., 2013; Kimura and Nakajima, 2014; Volker et al., 2014). Thus, it is envisaged that slightly depleted to enriched LILE compositions and relative depletion of selected HFSE in the studied samples are inherited from the parent basaltic melts derived through partial melting of a depleted mantle wedge metasomatized by influx of slab-dehydrated, LILE rich fluids (Saunders et al., 1980; Pearce et al., 1995; Aldanmaz et al., 2008; Ganguly et al., 2016).

The sub-arc mantle not only represents residues of basaltic melt extraction but also preserves evidence of compositional changes induced by melt impregnation, crystallization of silicate minerals and interaction between solid and liquid components of mantle melting (Pearce et al., 1999; Aldanmaz and Koprubasi, 2006). Slightly depleted LREE patterns in some of the studied ultramafic samples indicate progressive extraction of basaltic melt producing a refractory lithospheric mantle. During arc magmatism, the initial mantle melting and melt extraction episode is followed by chemical modification of the refractory mantle wedge by the fluids/melts derived from the subducting slab (Kerrick et al., 1998; Saha et al., 2015). However, the overall LREE enrichment of these rocks relative to HREE, the LREE/HREE and MREE/HREE fractionation trends are attributed to the modification of subduction zone mantle wedge by subduction components derived from ocean sediment and altered oceanic crust, transferred by melts derived from the subducted slab. Partial melting of metasomatized mantle wedge is held responsible for the observed relative enrichment of LILE and LREE with HFSE depletion in arc magmas (McCulloch and Gamble, 1991; Pearce et al., 2000). Accordingly, the sub-arc mantle wedge and fluids/melts derived from dehydrated subducted slab are potential contributors to arc magma sources, and their influence on subduction zone magmatism can be identified using distinct geochemical fingerprints preserved in the parent magmas and their derivatives (Perfit et al., 1980; Pearce and Peate, 1995; Maruyama et al., 2009). It has been advocated that mantle wedge metasomatism by silicate

melts primarily accounts for enrichment in LREE and to a lesser extent in highly incompatible elements like Th, U, Ba. Fluid metasomatism of mantle wedge does not affect LREE concentrations which are primarily controlled by impregnation of LREE enriched silicate melt fractions. Therefore, impregnation of sub-arc mantle wedge by silicate melts stands as the principal factor contributing to LREE enrichment over HREE in the studied gabbros. The geochemical signatures of the studied rocks provide evidence for involvement of both silicate melts and slab-dehydrated fluids in the process. The low Th/Ce ratios (0.003–0.322), high Ba/Nb (1.74–23.7) and Ba/Th (21.31–1567.1) ratios for these rocks suggest that the mantle source was probably metasomatized by slab fluids with minor melts derived from either subducted oceanic slabs or pelagic sediments (Hawkesworth et al., 1997).

On Nb/Yb vs. Th/Yb diagram (Fig. 17a; after Pearce, 2008) the plots of these gabbros are falling in the mantle array between N-MORB and E-MORB compositions and corresponding to the domain of active continental margins. The samples exhibit pronounced Nb-Ta positive anomalies in the primitive mantle-normalized multi-element diagrams which associate them with plume-related or asthenosphere-derived parent magmas containing Nb-Ta rich, recycled residual slab components (RSC). The fusion of

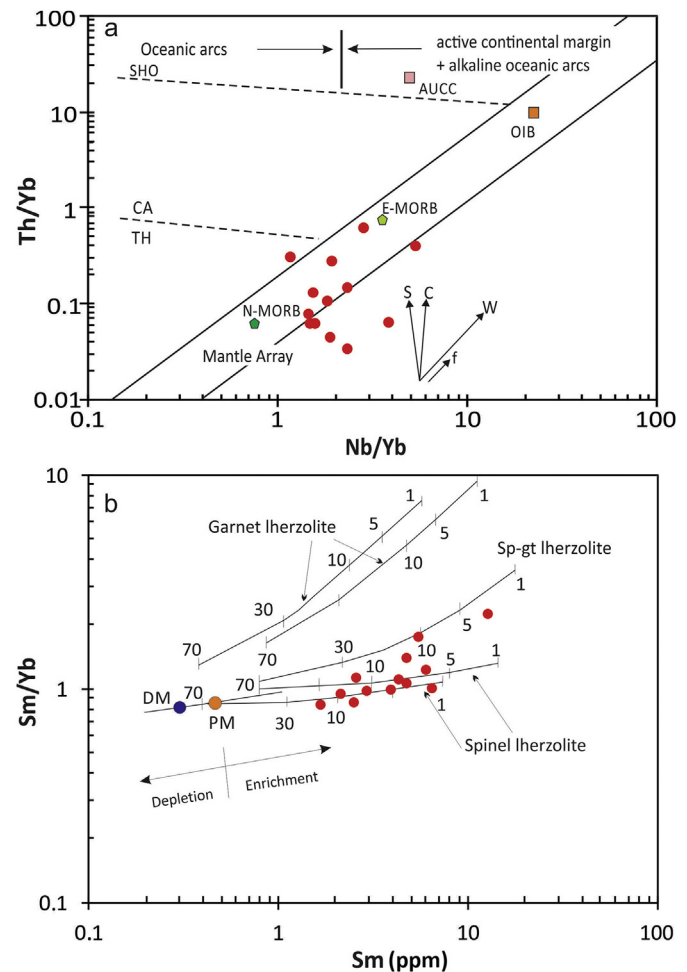
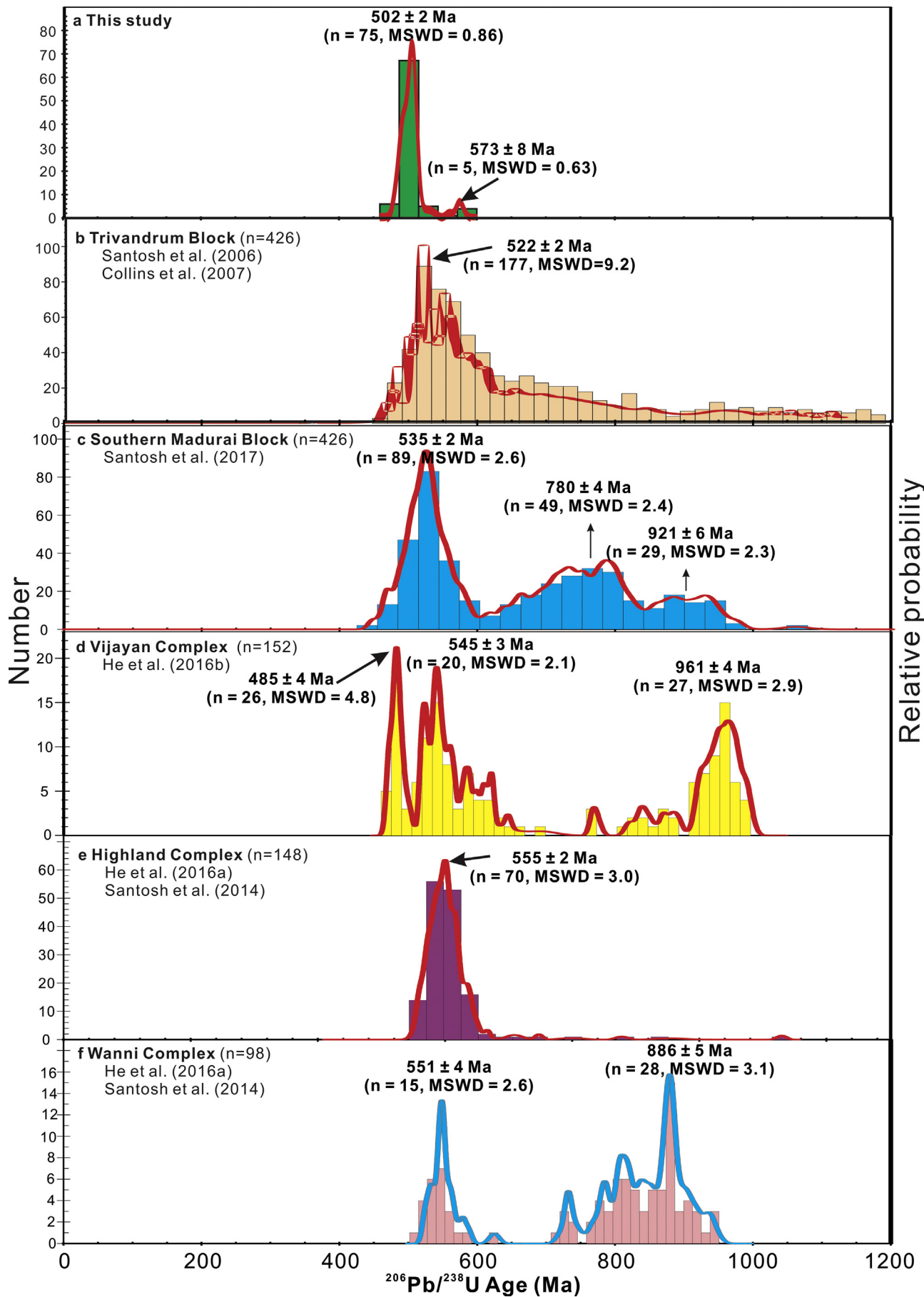


**Figure 17.** (a) Nb/Yb vs. Th/Yb (after Pearce, 2008) showing the plots of gabbros falling in the mantle array between N-MORB and E-MORB compositions and corresponding to the domain of active continental margins. Abbreviations: CA-calc-alkaline; TH-tholeiitic; SHO-shoshonite. (b) Sm/Yb vs. Sm plot (after Zhao and Zhou, 2007) corresponding to 5%–15% melting of spinel to spinel-garnet Iherzolite mantle. Melting curves are after Aldanmaz et al. (2000). DM and PM represents depleted and primitive mantle respectively. A pair of mode and melt mode curves are drawn for spinel Iherzolite (Kinzler, 1997) and garnet Iherzolite (Walter, 1998).



subducted slab-components by the upwelling of hot asthenospheric mantle through the slab window ensuing slab break-off during subduction-collision activities may be considered as another factor contributing to the elevated Nb abundances and positive Nb–Ta anomalies. In terms of Th–Nb–LREE compositions, the studied rocks with high Ce/Nb and low Th/Nb reflect the involvement of depleted MORB type mantle (DMM) in their genesis (Saunders et al., 1988; Safonova et al., 2008; Safonova, 2009). However, the variable  $(\text{Nb/La})_{\text{PM}}$ ,  $(\text{Nb/Th})_{\text{PM}}$ ,  $(\text{Th/Nb})_{\text{PM}}$  and  $(\text{Th/La})_{\text{PM}}$  ratios (Supplementary Table 1) collectively attest to contributions from subduction-derived component (SDC) in the melting process and suggest that parental melts for the studied volcanic rocks were derived from a chemically heterogeneous source that experienced extensive interaction between depleted MORB type mantle (DMM), subduction-derived components (SDC) and recycled residual slab component (RSC) under transitional geodynamic conditions marked by subduction processes at active continental margin followed by slab break-off, asthenospheric upwelling and mixing with sub-arc mantle wedge, continental collisions and post-collisional tectonics.

#### 7.4. HFSE–REE systematics: magma generation and melting conditions

The HFSE and REE, being resistant to alteration, serve as useful geochemical proxies to distinguish different possible melt sources for mantle-derived magmas (Erkank and Kable, 1976; Pearce and Norry, 1979; Le Roex et al., 1983). The enrichment-depletion characters of the mantle source are assessed in terms of HFSE concentrations and HFSE/HFSE ratios (Pearce and Parkinson, 1993; Pearce, 2008). The studied samples have higher Nb (3.4–30.2 ppm) and variable Zr (13–441 ppm) contents compared to the N-MORB ( $\text{Nb} = 2.33 \text{ ppm}$ ,  $\text{Zr} = 74 \text{ ppm}$ ) implying their generation from a depleted to enriched mantle source (Sun and McDonough, 1989). Metasomatism by melts/fluids released from the subducting slab and interaction between mantle wedge and asthenospheric melts (McKenzie, 1989; Gibson et al., 1995) are the possible models responsible for the formation of the enriched mantle source. Different mantle sources responsible for the generation of Cenozoic island arc lavas have been identified on the basis of Nb/Ta, Zr/Hf and Zr/Sm ratios (König and Schuth, 2011; Xiong et al., 2011) and these are (1) depleted MORB source in the sub-arc mantle wedge, (2) MORB like source with signatures of slab melts having rutile-eclogite residues of cold, deep slabs and (3) melts from hot shallow slabs having amphibole-garnet residue. The studied dykes have Zr/Hf (24.5–45.7) ratios greater than the primitive mantle value of 36, while Zr/Sm (7.1–16.5, except one sample having  $\text{Zr/Sm} = 34.3$ ) ratios are lower than the primitive mantle ( $\text{Zr/Sm} = 25$ ). The Nb/Ta ratios of the studied samples range from 3.5 to 7.4 in comparison with primitive mantle value of 17. These geochemical parameters are consistent flux-induced metasomatism of mantle wedge and crystallization of amphibole in the parent melt (Elliott et al., 1997; Munker et al., 2004). The fractionated Nb/Ta ratios with positive Nb–Ta anomalies on primitive mantle normalized multi-element diagram are consistent with greater garnet-melt and Cpx-melt partition coefficients under elevated pressures (20–75 kbar) and hydrous conditions (5–27 wt.%; Green et al., 2000). Klimm et al. (2008) suggested that accessory residual phases such as rutile, titanite and allanite in the source and their transport through fluids and hydrous melts control Nb/Ta

fractionation in arc system. According to Fulmer et al. (2010), amphibole plays a more important role at pressures 525 kbar in the Nb–Ta budget of subduction zone magmas generated under hydrous conditions. The fractionated Nb/Ta values for the studied gabbros are attributed to crystallization of amphibole from slab-derived, silica-rich aqueous fluids that fractionate Nb from Ta in the residual fluids. The Zr/Nb ratios of these rocks depict a wide range from 1.7 to 14.6 in conformity with that of N-MORB ( $\text{Zr/Nb} = 11$ –39) and recent oceanic primitive arc tholeiites ( $\text{Zr/Nb} = 9$ –87) thereby indicating depleted to enriched nature of the mantle wedge marked by interaction between depleted mantle and subduction-derived fluids and melts (Sun and McDonough, 1989; Pearce and Peate, 1995). Nd–Hf compositions of arc magmas reveal that in comparison with Hf, Nd behaves as a mobile element in slab-derived fluids/melts. It has been suggested that subduction-metasomatized mantle wedge have increased concentrations of Nd compared to Hf. The LREE–HFSE chemistry of rocks is marked by elevated abundances of Nd with relative Hf depletion resulting into high Nd/Hf ratios ranging from 5.5 to 15.6, indicative of metasomatic overprints of mantle wedge melts, were controlled by addition of slab derived fluids and melts. Elevated Ba/Th ratios suggest contributions from both subducted slab sediments and aqueous fluids released by slab dehydration (McCulloch and Gamble, 1991; Elliott et al., 1997; Elburg et al., 2002; Stern, 2002). Therefore, the subduction signatures in these rocks reflect a combination both fluids and sediment input as also observed in the Late Paleozoic volcanic rocks from western Chinese Tianshan (Yang et al., 2014). Geochemical signatures of modern arc-related magmatism suggest that Ba/Nb ratio is an effective geochemical proxy indicating the fluid/water content in the mantle source, while Ba/La can be used as a tracer for the total slab-derived input into the mantle wedge (Cervantes and Wallace, 2003; Yang et al., 2014). The Ba/Nb ratios for the studied samples ranging from 1.7 to 23.7 corroborate the presence of hydrous minerals (e.g. phlogopite or amphibole) in the source region, while their Ba/La (3–41) ratios reflect metasomatism of refractory mantle wedge by variable inputs from slab-derived fluids, melts and sediments augmenting strong subduction overprints in the resultant magmas (Carr et al., 1990; Patino et al., 2000; Jenner et al., 2009).

Rare-earth element compositions are sensitive to mantle melting conditions and provide important constraints in understanding the degree and depth of partial melting because their relative abundances in mantle-derived melts are strongly dependent on the extent of partial melting and the nature of aluminous phase (spinel or garnet) occurring in the mantle source of peridotitic composition (Lassiter et al., 1995; Reichow et al., 2005; He et al., 2010; Manikyamba et al., 2015). The higher distribution coefficients of HREE (Yb) and Y for garnet account for their dominant control over the degree and depth of mantle melting (Song et al., 2006). However, La, Sm and Gd are incompatible and have low garnet/melt partition coefficients (Irving and Frey, 1978; Kelemen, 1990; Rollinson, 1993). La/Yb is strongly fractionated when melting occurs in the garnet stability field and slightly fractionated during melting in the spinel lherzolite domain (Yaxley, 2000; Xu et al., 2005; Lai et al., 2012). The La/Yb ratio gives a measure of LREE/HREE fractionation and is particularly sensitive to the amount of garnet left in the restite which in turn reflects the degree of melting of a garnet lherzolite source (Condé, 2001). The studied mafic dykes have  $(\text{La/Yb})_{\text{N}}$  ratios ranging from 0.65 to 3.5 that corroborate feeble to pronounced LREE/HREE fractionation

**Figure 18.** Combined age data histograms of the various crustal blocks in southern India and Sri Lanka showing the major age peaks. Note the youngest age peaks for the gabbroic rocks of present study corresponding to post-collisional magmatism, distinct from the other late Neoproterozoic age peaks in the various blocks associated with subduction and collision. Data for Trivandrum Block and Achankovil Shear Zone after Santosh et al. (2006) and Collins et al. (2007), for southern Madurai Block after Santosh et al. (2017), and for the Sri Lankan blocks after Santosh et al. (2014), He et al. (2016a,b).

corresponding to low degree melting in a mantle regime having spinel to garnet lherzolitic composition. The La/Sm ratios for the studied samples ranging from 0.5 to 2.43 indicate that the melting domain extended over a variable depth range from the stability field of spinel to garnet with respective occurrence of spinel and garnet as stable phase in the mantle restite. Sm/Yb ratio can be a useful tool to constrain the mantle source mineralogy, for Sm, being an incompatible element, is affected significantly by variation in the source mineralogy (e.g., garnet or spinel), whereas Yb is compatible with garnet but not with clinopyroxene or spinel (Aldanmaz et al., 2000; Zhao and Zhou, 2007; Liu et al., 2012). Sm/Yb ratios of spinel-lherzolite source partial melts are similar to those of mantle and thus, form a horizontal melting trend that lies within, or close to, a mantle array defined by depleted mantle (DM, McKenzie and O’Nions, 1991) and enriched subcontinental lithospheric mantle (SCLM, Aldanmaz et al., 2000). On the other hand, partial melts from a garnet-lherzolite source (with garnet residue) will have significantly higher Sm/Yb ratios than mantle source. The studied rocks have Sm/Yb ratios varying between 0.96 and 2.53 implying a mantle source of spinel-garnet lherzolite. On Sm/Yb vs. Sm plot (Fig. 17b, after Zhao and Zhou, 2007) the samples are falling on the melting curves of spinel lherzolite and extending up to the spinel-garnet lherzolite melting domain thereby reflecting 5%–15% melting of spinel to spinel-garnet lherzolite mantle. Further, relatively low Ce/Y ratios (<2) for these rocks (0.24–1.04) suggest that the parent melts were generated within the spinel-garnet stability at a depth of approximately 60–80 km (McKenzie and Bickle, 1988). Dy/Yb ratio is considered as an important geochemical proxy to distinguish between the spinel and garnet stability fields during partial melting (Jiang et al., 2009; Yang et al., 2014). Partial melting in the garnet stability field results into high Dy/Yb ratios (>2.5), whereas melting in the spinel stability field accounts for low Dy/Yb ratios (<1.5). The Dy/Yb ratios for the studied gabbros (1.3–2.13) commensurate with mantle melting under spinel-garnet facies condition. Furthermore, Gd/Yb ratios for these rocks (1.03–2.3) attest to melting of spinel and garnet lherzolite mantle sources.

### 7.5. Implications of trace element and U–Pb age data

The zircon grains from the gabbros show patchy or striped zoning with only few gains displaying faint oscillatory zoning typical of zircon grains in mafic magmatic rocks. Their low U and Pb content are also typical of zircon grains crystallizing from mafic magmas. Zircon is considered to be relatively rare or absent in mafic and ultramafic rocks, although several studies have reported zircon grains even in ultramafic rocks such as peridotites, pyroxenites and in kimberlites (Rudnick et al., 1999; Bea et al., 2001; Katayama et al., 2003; Yang et al., 2016a,b). The formation of zircon grains in such cases have been correlated to melt-peridotite metasomatism (Liu et al., 2012) with Zr supplied by the infiltration of subduction zone fluids. Zircon crystallized through such process where plagioclase is also a crystallizing phase would display prominent positive Ce and negative Eu anomalies (e.g., Liu et al., 2012; Hu et al., 2017).

Among the zircon grains from three samples analyzed in this study, those in samples PG-6 and PG-17 show a single major population that yields concordant age data and  $^{206}\text{Pb}/^{238}\text{U}$  mean age of 507–494 Ma. The major age peak in the third sample (PG-15) is also similar at 505 Ma, but this rock also carries another older population of xenocrystic zircons that yield a mean age of 573 Ma. The zircon U–Pb age data clearly show that the gabbroic magma was emplaced during Cambrian.

In Fig. 18 we compile the available age data from various crustal blocks/units in southern India (Trivandrum, Achankovil, Southern Madurai) and the adjacent terranes in Sri Lanka (Wanni, Vijayan,

Highland and Kadugannawa) and compare these with the results from our study. The Trivandrum Block and Achankovil Shear Zone data include metasediments with detrital zircon sourced from multiple age provenance, although both data also reveal the prominent Late Neoproterozoic age peak corresponding to regional metamorphism associated with the assembly of Gondwana. The southern Madurai Block shows prominent Neoproterozoic age peaks related to prolonged arc magmatism associated with subduction before the final collisional assembly. Blocks in Sri Lanka share a similar history during the Neoproterozoic, culminating in latest Neoproterozoic–Cambrian ages associated with Gondwana assembly.

However, the late Cambrian ages of the gabbroic rocks dated in this study are distinct, and younger than the ages related to the magmatic and metamorphic ages of the Neoproterozoic subduction-collision events in all these terranes. A similar age peak is also present in the Vijayan Complex of Sri Lanka. Thus, the age data clearly indicate that the mafic magmatism reported in this study occurred in a post-collisional setting, possibly during orogenic collapse and extension following the assembly of Gondwana, with magmatism aided by asthenospheric upwelling in response to slab break-off.

In Fig. 19 we show a schematic plate tectonic sketch to illustrate the subduction-collision and post-collisional extension with slab break-off triggering asthenospheric upwelling and mafic magmatism. The continental block to the north is represented by the Madurai Block and to the south is the Nagercoil Block. The metasediments in the khondalite belt of Trivandrum Block is envisaged as an accretionary complex that also involves fragments of Paleoproterozoic basement. This model is consistent with the

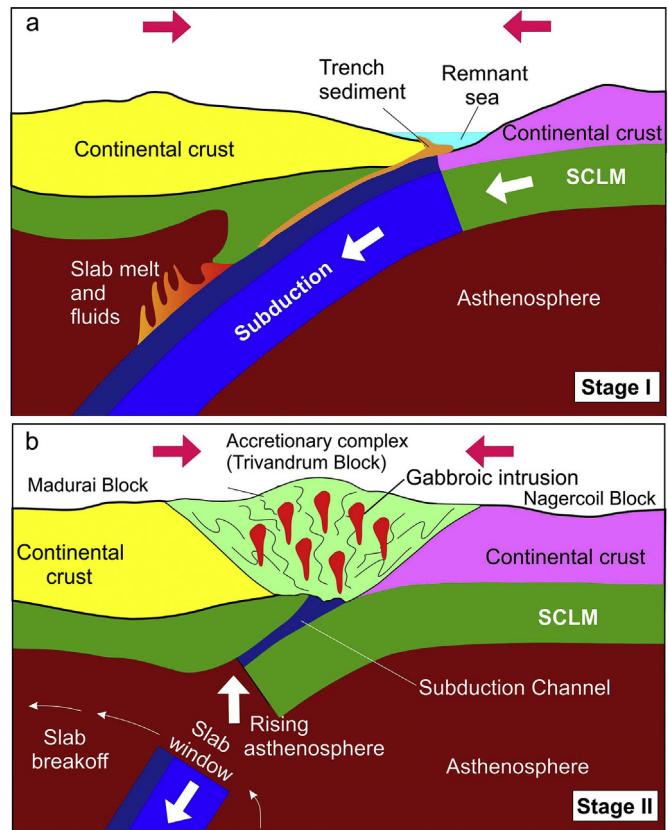


**Figure 19.** Schematic plate tectonic model illustrating (a) subduction-accretion during Neoproterozoic; and (b) collision, slab break-off, asthenospheric upwelling and emplacement of gabbroic magma in the Trivandrum Block. See text for explanation.

geochemical and geochronological data presented in this study suggesting asthenospheric input in mafic magmatism within a post-collisional setting.

## 8. Conclusions

The suite of gabbro dykes and sills intruding granulite facies metapelites of the Trivandrum Block are characterized by the dominant assemblage of clinopyroxene-plagioclase. Their overall major oxide compositions suggest that the evolution of parental melts was dominantly controlled by fractional crystallization. The rocks show enrichment of LILE and LREE and depletion of relative to typical primitive mantle values with negative anomalies at Zr-Hf and Ti suggesting subduction zone magmatic regime. Geochemical features suggest transition from arc to intraplate affinity with parental melts derived from heterogeneous sources and magma emplacement under subduction to post-collisional settings. The gabbros straddle the mantle array between N-MORB and E-MORB compositions and correspond to the domain of active continental margins. Trace element data suggest low degree melting in a mantle regime having spinel to garnet Iherzolitic composition. The zircon grains from the gabbros show magmatic crystallization textures with low U and Pb content. They yield  $^{206}\text{Pb}/^{238}\text{U}$  mean age of 507–494 Ma with one sample carrying additional xenocrystic zircons with a mean age of 573 Ma. The zircon U-Pb age data clearly show that the gabbroic magma was emplaced during Cambrian. The Cambrian ages of the gabbroic rocks dated in this study are distinct, and younger than the ages related to the magmatic and metamorphic ages of the Neoproterozoic subduction-collision events in all these terranes. A similar age peak is also present in the Vijayan Complex of Sri Lanka. Thus, the age data clearly indicate that the mafic magmatism reported in this study occurred in a post-collisional setting, possibly during orogenic collapse and extension following the assembly of Gondwana, with magmatism aided by asthenospheric upwelling in response to slab break-off.

## Acknowledgments

We thank Associate Editor Prof. Sanghoon Kwon, Referee Dr. Vinod Samuel and another anonymous reviewer for their constructive comments. This study was funded by Foreign Expert grants to M. Santosh from the China University of Geosciences, Beijing. The authors thank Dr. S. Anirudhan, Professor and Head, Department of Geology, University of Kerala for his encouragements. We thank Director, CESS, and Dr. G.R. Ravindra Kumar Scientist, CESS, Akkulam, Trivandrum for providing XRF facility. SG acknowledges DST INSPIRE Faculty project [IFA 14-EAS-25] for financial support.

## Appendix A. Supplementary data

Supplementary data related to this article can be found at <https://doi.org/10.1016/j.gsf.2017.12.002>.

## References

- Aldanmaz, E., Koprubasi, N., 2006. Platinum-group-element systematics of peridotites from Ophiolite Complexes of Northwest Anatolia, Turkey: implications for mantle metasomatism by Melt Percolation in a supra-subduction zone environment. *International Geology Reviews* 48 (5), 420–442.
- Aldanmaz, E., Pearce, J., Thirlwall, M., Mitchell, J., 2000. Petrogenetic evolution of late Cenozoic, post-collision volcanism in western Anatolia, Turkey. *Journal of Volcanology and Geothermal Research* 102, 67–95.
- Aldanmaz, E., Yaliniz, M.K., Guctekin, A., Goncuoglu, M.C., 2008. Geochemical characteristics of mafic lavas from the Neotethyan ophiolites in western Turkey: implications for heterogeneous source contribution during variable stages of ocean crust generation. *Geological Magazine* 145, 37–54.
- Andersen, T., 2002. Correction of common lead in U-Pb analyses that do not report  $^{204}\text{Pb}$ . *Chemical Geology* 192, 59–79.
- Bea, F., Fershtater, G.B., Montero, P., Whitehouse, M., Levin, V.Y., Scarrow, J.H., Austrheim, H., Pushkariev, E.V., 2001. Recycling of continental crust into the mantle as revealed by Kytylym dunite zircons, Ural Mts, Russia. *Terra Nova* 13, 407–412.
- Bindu, R.S., Suzuki, K., Yoshida, M., Santosh, M., 1998. The first report of CHIME monazite age from the south Indian granulite terrain. *Current Science* 74, 852–858.
- Bourdon, E., Eissen, J.-P., Monzier, M., Robin, C., Martin, H., Cotten, J., Hall, M.L., 2002. Adakite-like lavas from Antisana Volcano (Ecuador): evidence for slab melt metasomatism beneath the Andean Northern volcanic zone. *Journal of Petrology* 43, 199–217.
- Cabral, R.A., Jackson, M.G., Rose-Koga, E.F., Koga, K.T., Whitehouse, M.J., Antonelli, M.A., Farquhar, J., Day, J.M.D., Hauri, E.H., 2013. Anomalous sulphur isotopes in plume lavas reveal deep mantle storage of Archaean crust. *Nature* 496, 490–494.
- Carlson, R.W., 1991. Physical and chemical evidence on the cause and source characteristics of flood-basalt volcanism. *Australian Journal of Earth Sciences* 38, 525–544.
- Carlson, R.W., Hart, W.K., 1988. Flood basalt volcanism in the Northwestern United States. In: Macdougall, J.D. (Ed.), *Continental Flood Basalts*. Kluwer Academic Publication, Dordrecht, pp. 35–61.
- Carr, M.J., Feigenson, M.D., Bennett, E.A., 1990. Incompatible element and isotopic evidence for tectonic control of source mixing and melt extraction along the Central-American arc. *Contributions to Mineralogy and Petrology* 105, 369–380.
- Cervantes, P., Wallace, P.J., 2003. Role of  $\text{H}_2\text{O}$  in subduction-zone magmatism: new insights from melt inclusions in high-Mg basalts from central Mexico. *Geology* 31, 235–238.
- Chacko, T., Ravindra Kumar, G.R., Newton, R.C., 1987. Metamorphic P-T conditions of Kerala (South India) Khondalite Belt, a granulite facies supracrustal terrain. *The Journal of Geology* 95, 343–358.
- Chetty, T.R.K., Rao, Y.J.B., 2006. The Cauvery shear zone, Southern Granulite Terrain, India: a crustal-scale flower structure. *Gondwana Research* 10, 77–85.
- Clark, C., Collins, A.S., Timms, N.E., Kinny, P.D., Santosh, M., 2009. SHRIMP U-Pb age constraints on magmatism and high-grade metamorphism in the Salem Block, southern India. *Gondwana Research* 16, 27–36.
- Clark, C., Healy, D., Johnson, T., Collins, A.S., Taylor, T.J., Santosh, M., Timms, N.E., 2015. Hot orogens and supercontinent amalgamation: a Gondwanan example from southern India. *Gondwana Research* 28, 1310–1328.
- Collins, A.S., Clark, C., Plavsa, D., 2014. Peninsular India in Gondwana: the tectono-thermal evolution of the southern granulite terrain and its Gondwanan counterparts. *Gondwana Research* 25, 190–203.
- Collins, A.S., Santosh, M., Braun, I., Clark, C., 2007. Age and sedimentary provenance of the southern granulites, south India: U-Th-Pb SHRIMP. *Precambrian Research* 155, 125–138.
- Condie, K.C., 2001. *Mantle Plumes and Their Record in Earth History*. Cambridge University Press, London, p. 305.
- Condie, K.C., 2003. Incompatible element ratios in oceanic basalts and komatiites: tracking deep mantle sources and continental growth rates with time. *Geochemistry, Geophysics, Geosystems* 4, 2002GC000333.
- Conrad, C.P., Molnar, P., 1999. Convective instability of a boundary layer with temperature-and strain-rate-dependent viscosity in terms of ‘available buoyancy’. *Geophysical Journal International* 139, 51–68.
- Cox, K.G., Bell, J.D., Pankhurst, R.J., 1979. *The Interpretation of Igneous Rocks*. George, Allen and Unwin, London, p. 450.
- Davies, J.H., von Blanckenburg, F., 1995. Slab breakoff: a model of lithosphere detachment and its test in the magmatism and deformation of collisional orogens. *Earth and Planetary Science Letters* 129, 85–102.
- Defant, M.J., Drummond, M.S., 1990. Derivation of some modern arc magmas by melting of young subducted lithosphere. *Nature* 347, 662–665.
- DePaolo, D.J., 1981. Trace element and isotopic effects of combined wallrock assimilation and fractional crystallisation. *Earth and Planetary Science Letters* 53, 189–202.
- Dilek, Y., Furnes, H., Shallo, M., 2008. Geochemistry of the Jurassic Mirdita Ophiolite (Albania) and the MORB to SSZ evolution of a marginal basin oceanic crust. *Lithos* 100, 174–209.
- Dokuz, A., 2011. A slab detachment and delamination model for the generation of Carboniferous high-potassium I-type magmatism in the Eastern Pontides, NE Turkey: the Köse composite pluton. *Gondwana Research* 19, 926–944.
- Elburg, A.M., van-Bergen, V.M., Hoogewerff, J., Foden, J., Vroon, P., Zulkarnain-Iskandar, I., Nasution-Asnawir, A., 2002. Geochemical trends across an arc-continent collision zone: magma sources and slab-wedge transfer processes below the Pantar Strait volcanoes, Indonesia. *Geochimica et Cosmochimica Acta* 66, 2771–2789.
- Elliott, T., Plank, T., Zindler, A., White, W., Bourdon, B., 1997. Element transport from slab to volcanic front at the Mariana arc. *Journal of Geophysical Research* 102, 14991–15019.
- Erlank, A.J., Kable, E.J.D., 1976. The significance of incompatible elements in Mid-Atlantic Ridge basalts from  $45^{\circ}$  N, with particular reference to Zr/Nb. *Contributions to Mineralogy and Petrology* 54, 281–291.
- Ewart, A., Collerson, K.D., Regelous, M., Wendt, J.I., Ni, Y., 1998. Geochemical evolution within the Tonga–Kermadec–Lau arc–back-arc systems: the role of varying mantle wedge composition in space and time. *Journal of Petrology* 39, 331–368.
- Fei, H., Wiedenbeck, M., Yamazaki, D., Katsura, T., 2013. Small effect of water on upper-mantle rheology based on silicon self diffusion coefficients. *Nature* 498, 213–216.

- Ferrari, L., 2004. Slab detachment and control on mafic volcanic pulse and mantle heterogeneity in Central Mexico. *Geology* 32, 77–80.
- Foley, S., Tiepolo, M., Vannucci, R., 2002. Growth of early continental crust controlled by melting of amphibolite in subduction zones. *Nature* 417, 837–840.
- Fulmer, E.C., Nebel, O., van Westrenen, W., 2010. High-precision high field strength element partitioning between garnet, amphibole and alkaline melt from Kakanui, New Zealand. *Geochimica et Cosmochimica Acta* 74, 2741–2759.
- Gallagher, K., Hawkesworth, C.J., 1992. Dehydration melting and generation of continental flood-basalts. *Nature* 358, 57–59.
- Ganguly, S., Manikyamba, C., Saha, A., Lingadevaru, M., Santosh, M., Rambabu, S., Khelen, A.C., Purushotham, D., Linga, D., 2016. Geochemical characteristics of gold bearing boninites and banded iron formations from Shimoga greenstone belt, India: implications for gold genesis and hydrothermal processes in diverse tectonic settings. *Ore Geology Reviews* 73, 59–82.
- Gerya, T.V., Yuen, D.A., Maresch, W.V., 2004. Thermomechanical modelling of slab detachment. *Earth and Planetary Science Letters* 226, 101–116.
- Gibson, S.A., Thompson, R.N., Leonards, O.H., Dickin, A.P., Mitchell, J., 1995. The Late Cretaceous impact of the Trindade Mantle Plume: evidence from large-volume, mafic, potassic magmatism in SE Brazil. *Journal of Petrology* 36, 189–229.
- Green, T.H., Blundy, J.D., Adam, J., Yaxley, G.M., 2000. SIMS determination of trace element partition coefficients between garnet, clinopyroxene and hydrous basaltic liquids at 2–7.5 GPa and 1080–1200 °C. *Lithos* 53, 165–187.
- Harley, S.L., Nandakumar, V., 2016. New evidence for Palaeoproterozoic high grade metamorphism in the Trivandrum Block, Southern India. *Precambrian Research* 280, 120–138.
- Hawkesworth, C.J., Rogers, N.W., Vancalsteren, P.W.C., 1984. Mantle enrichment processes. *Nature* 311, 331–335.
- Hawkesworth, C.J., Turner, S.P., McDermott, F., Peate, D.W., van Calsteren, P., 1997. U–Th isotopes in arc magmas: implications for element transfer from the subducted crust. *Science* 276, 551–555.
- He, Q., Xiao, L., Balta, B., Gao, R., Chen, J., 2010. Variety and complexity of the Late-Permian Emeishan basalts: reappraisal of plume-lithosphere interaction process. *Lithos* 119, 91–107.
- He, X.F., Santosh, M., Tsunogae, T., Malaviarachchi, S.P.K., 2016a. Early to late Neoproterozoic magmatism and magma mixing-mingling in Sri Lanka: implications for convergent margin processes during Gondwana assembly. *Gondwana Research* 32, 151–180.
- He, X.F., Santosh, M., Tsunogae, T., Malaviarachchi, S.P.K., Dharmapriya, P.L., 2016b. Neoproterozoic arc accretion along the 'eastern suture' in Sri Lanka during Gondwana assembly. *Precambrian Research* 279, 57–80.
- Hergt, J., Peate, D., Hawkesworth, C.J., 1991. The petrogenesis of Mesozoic Gondwana low Ti fold basalts. *Earth and Planetary Science Letters* 105, 134–148.
- Hofmann, A.W., 1997. Mantle geochemistry: the message from oceanic volcanism. *Nature* 385, 219–229.
- Houseman, G.A., McKenzie, D.P., Molnar, P., 1981. Convective instability of a thickened boundary layer and its relevance for the thermal evolution of continental convergent belts. *Journal of Geophysical Research* 86, 6115–6132.
- Hu, C.N., Santosh, M., Yang, Q.Y., Kim, S.W., Nakagawa, M., Maruyama, S., 2017. Magmatic and metasomatic imprints in a long-lasting subduction zone: evidence from zircon in rodilite and serpentinite of Kochi, SW Japan. *Lithos* 274–275, 349–362.
- Irvine, T.N., Baragar, W.R.A., 1971. A guide to the chemical classification of the common volcanic rocks. *Canadian Journal of Earth Sciences* 8, 523–548.
- Irving, A.J., Frey, F.A., 1978. Distribution of trace elements between garnet megacrysts and host volcanic liquids of kimberlitic to rhyolitic composition. *Geochimica et Cosmochimica Acta* 42, 771–787.
- Iwamori, H., Nakamura, H., 2015. Isotopic heterogeneity of oceanic, arc and continental basalts and its implications for mantle dynamics. *Gondwana Research* 27, 1131–1152.
- Jenner, F.E., Bennett, V.C., Nutman, A.P., Friend, C.R.L., Norman, M.D., Yaxley, G., 2009. Evidence for subduction at 3.8 Ga: geochemistry of arc-like metabasalts from the southern edge of the Isua Supracrustal Belt. *Chemical Geology* 261, 82–97.
- Jensen, L.S., 1976. A New Cation Plot for Classifying Sub-alkaline Volcanic Rocks. *Miscellaneous Papers, Ontario Division of Mines*, MP66, p. 22.
- Jiang, Y.H., Jiang, S.Y., Dai, B.Z., Liao, S.Y., Zhao, K.D., Ling, H.F., 2009. Middle to late Jurassic felsic and mafic magmatism in southern Hunan province, southeast China: implications for a continental arc to rifting. *Lithos* 107, 185–204.
- Katayama, I., Hirose, K., Yurimoto, H., Nakashima, S., 2003. Water solubility in majoritic garnet in subducting oceanic crust. *Geophysical Research Letters* 30. <https://doi.org/10.1029/2003GL018127>.
- Kay, R.W., Kay, S.M., 1993. Delamination and delamination magmatism. *Tectonophysics* 219, 177–189.
- Kellemen, P., 1990. Reaction between ultramafic rock and fractionating basaltic liquid I. Phase relations, the origin of calc-alkaline magma series, and the formation of discordant dunite. *Journal of Petrology* 31, 51–98.
- Kerrick, R., Wyman, D., Fan, J., Bleeker, W., 1998. Boninite series: low Ti-tholeiite association from the 2.7 Ga Abitibi greenstone belt. *Earth and Planetary Science Letters* 164, 303–316.
- Keskin, M., 2003. Magma generation by slab steepening and break off beneath a subduction-accretion complex: an alternative model for collision-related volcanism in Eastern Anatolia, Turkey. *Geophysical Research Letters* 30, 8046–8049.
- Keskin, M., 2007. Eastern Anatolia: a hotspot in a collision zone without a mantle plume. In: Fouger, G., Jurdy, D.M. (Eds.), *Plates, Plumes and Planetary Processes*. Geological Society of America, Colorado, pp. 693–722.
- Kimura, J., Yoshida, T., 2006. Contributions of slab fluid, mantle wedge and crust to the origin of quaternary lavas in the NE Japan arc. *Journal of Petrology* 47 (11), 2185–2232.
- Kimura, J.-I., Nakajima, J., 2014. Behaviour of subducted water and its role in magma genesis in the NE Japan arc: a combined geophysical and geochemical approach. *Geochimica et Cosmochimica Acta* 143, 165–188.
- Kinzler, R.J., 1997. Melting of mantle peridotite at pressures approaching the spinel to garnet transition: application to midocean ridge basalt petrogenesis. *Journal of Geophysical Research* 102, 853–874.
- Klimm, K., Blundy, J.D., Green, T.H., 2008. Trace element partitioning and accessory phase saturation during  $H_2O$ -saturated melting of basalt with implications for subduction zone chemical fluxes. *Journal of Petrology* 49, 523–553.
- Konig, S., Munker, C., Schuth, S., Luguet, A., Hoffmann, J.E., Kudoon, J., 2010. Boninites as windows into trace element mobility in subduction zones. *Geochimica et Cosmochimica Acta* 74, 684–704.
- Konig, S., Schuth, S., 2011. Deep melting of old subducted oceanic crust recorded by superchondritic Nb/Ta in modern island arc lavas. *Earth and Planetary Science Letters* 301, 265–274.
- Krishna, A.K., Murthy, N.N., Govil, P.K., 2007. Multi-element analysis of soils by wavelength-dispersive X-ray fluorescence spectrometry. *Atomic Spectroscopy* 28, 202–214.
- Kröner, A., Santosh, M., Hegner, E., Shaji, E., Nanda-Kumar, V., 2015. Palaeoproterozoic ancestry of Pan-African high-grade granitoids in southernmost India: implications for Gondwana reconstructions. *Gondwana Research* 27, 1–37.
- Krystopowicz, N.J., Currie, C.A., 2013. Crustal eclogitization and lithosphere delamination in orogens. *Earth and Planetary Science Letters* 361, 195–207.
- Lai, S., Qin, J., Li, Y., Li, S., Santosh, M., 2012. Permian high Ti/Y basalts from the eastern part of the Emeishan Large Igneous Province, southwestern China: petrogenesis and tectonic implications. *Journal of Asian Earth Sciences* 47, 216–230.
- Lassiter, J.C., DePaolo, D.J., Mahoney, J.J., 1995. Geochemistry of the Wrangelia Flood Basalt Province: implications for the role of continental and oceanic lithosphere in Flood Basalt Genesis. *Journal of Petrology* 36, 983–1009.
- Le Roex, A.P., Dick, H.J.B., Erlank, A.J., Reid, A.M., Frey, F.A., Hart, S.R., 1983. Geochemistry, mineralogy and petrogenesis of lavas erupted along the Southwest Indian Ridge between the Bouvet Triple Junction and 11 degrees east. *Journal of Petrology* 24 (3), 267–318.
- Liao, F., Chen, N., Santosh, M., Wang, Q., Gong, S., He, C., Mustafa, H.A., 2018. Paleoproterozoic Nb-enriched meta-gabbros in the Quanji Massif, NW China: implications for assembly of the Columbia supercontinent. *Geoscience Frontiers* 9 (2), 577–590.
- Lightfoot, P.C., Hawkesworth, C.J., Hergt, J., Naldrett, A.J., Gorbachev, N.S., Fedorenko, V.A., Doherty, W., 1993. Remobilisation of the continental lithosphere by a mantle plume: major-, trace-element, and Sr-, Nd-, and Pb-isotope evidence from picritic and tholeiitic lavas of the Noril'sk District, Siberian Trap, Russia. *Contributions to Mineralogy and Petrology* 114, 171–188.
- Liu, S., Kröner, A., Wan, Y., Santosh, M., Shaji, E., Dhanil Dev, S.G., 2016. Late Palaeoproterozoic depositional age for khondalite protoliths in southern India and tectonic implications. *Precambrian Research* 283, 50–67.
- Liu, S., Zhang, J., Li, Q., Zhang, L., Wang, W., Yang, P., 2012. Geochemistry and U–Pb zircon ages of metamorphic volcanic rocks of the Paleoproterozoic Luliang Complex and constraints on the evolution of the Trans-North China Orogen, North China Craton. *Precambrian Research* 222–223, 173–190.
- Ludwig, K.R., 2003. User's Manual for Isoplot/Ex v3.0, a Geochronology Toolkit for Microsoft Excel. In: Berkeley Geochronological Center Special Publications, vol. 4, pp. 25–31.
- Mahoney, J.J., 1988. Deccan traps. In: Macdougall, J.D. (Ed.), *Continental Flood Basalts*. Kluwer, Dordrecht, pp. 151–194.
- Manikyamba, C., Ray, J., Ganguly, S., Rajanikanta Singh, M., Santosh, M., Saha, A., Satyanarayanan, M., 2015. Boninitic metavolcanic rocks and island arc tholeiites from the Older Metamorphic Group (OMG) of Singhbhum Craton, eastern India: geochemical evidence for Archean subduction processes. *Precambrian Research* 271, 138–251.
- Maruyama, S., Hasegawa, A., Santosh, M., Kogiso, T., Omori, S., Nakamura, H., Kawai, K., Zhao, D., 2009. The dynamics of big mantle wedge, magma factory, and metamorphic–metasomatic factory in subduction zones. *Gondwana Research* 16, 414–430.
- McCulloch, M.T., 1993. The role of subducted slabs in an evolving earth. *Earth and Planetary Science Letters* 115, 89–100.
- McCulloch, M.T., Gamble, A.J., 1991. Geochemical and geodynamical constraints on subduction zone magmatism. *Earth and Planetary Science Letters* 102, 358–374.
- McDonough, W.F., 1990. Constraints on the composition of the continental lithospheric mantle. *Earth and Planetary Science Letters* 101, 1–18.
- McKenzie, D., 1989. Some remarks on the movement of small melt fractions in the mantle. *Earth and Planetary Science Letters* 95, 53–72.
- McKenzie, D., Bickle, M.J., 1988. The volume and composition of melt generated by extension of the lithosphere. *Journal of Petrology* 29, 625–679.
- McKenzie, D.A.N., O'Nions, R.K., 1991. Partial melt distributions from inversion of rare earth element concentrations. *Journal of Petrology* 32, 1021–1091.

- Molnar, P., Houseman, G.A., Conrad, C.P., 1998. Rayleigh-Taylor instability and convective thinning of mechanically thickened lithosphere: effects of non-linear viscosity decreasing exponentially with depth and of horizontal shortening of the layer. *Geophysical Journal International* 133, 568–584.
- Mullen, E.D., 1983. MnO/TiO<sub>2</sub>/P<sub>2</sub>O<sub>5</sub>: a minor element discriminant for basaltic rocks of oceanic environments and its implications for petrogenesis. *Earth and Planetary Science Letters* 62, 53–62.
- Muller, D., Rock, N.M.S., Groves, D.I., 1992. Geochemical discrimination between shoshonitic and potassic volcanic rocks in different tectonic settings: a pilot study. *Mineralogy and Petrology* 46, 259–289.
- Munker, C., Wörner, G., Ygodzinski, G., Chrikova, T., 2004. Behaviour of high field strength elements in subduction zones: constraints from Kamchatka–Aleutian arc lavas. *Earth and Planetary Science Letters* 224, 275–293.
- Patino, L.C., Carr, M.J., Feigenson, M.D., 2000. Local and regional variations in Central American arc lavas controlled by variations in subducted sediment input. *Contributions to Mineralogy and Petrology* 138, 265–283.
- Pearce, J.A., Parkinson, I.J., 1993. Trace Element Models for Mantle Melting: Application to Volcanic Arc Petrogenesis. In: Geological Society of London Special Publication, vol. 76, pp. 373–403.
- Pearce, J.A., Kempton, P.D., Nowell, G.M., Noble, S.R., 1999. Hf–Nd element and isotope perspective on the nature and provenance of mantle and subduction components in Western Pacific arc-basin systems. *Journal of Petrology* 40, 1579–1611.
- Pearce, J.A., Baker, P.E., Harvey, P.K., Luff, I.W., 1995. Geochemical evidence for subduction fluxes, mantle melting and fractional crystallisation beneath the South Sandwich island arc. *Journal of Petrology* 36, 1073–1109.
- Pearce, J.A., 2008. Geochemical fingerprinting of oceanic basalts with applications to ophiolite classification and the search for Archean oceanic crust. *Lithos* 100, 14–48.
- Pearce, J.A., Barker, P.F., Edwards, S.J., Parkinson, I.J., 2000. Geochemistry and tectonic significance of peridotites from the South Sandwich arc–basin system, South Atlantic. *Contributions to Mineralogy and Petrology* 139, 36–53.
- Pearce, J.A., Norry, M.J., 1979. Petrogenetic implications of Ti, Zr, Y and Nb variations in volcanic rocks. *Contributions to Mineralogy and Petrology* 69, 33–47.
- Pearce, J.A., Peate, D.W., 1995. Tectonic implications of the composition of volcanic arc magmas. *Annual Review of Earth and Planetary Sciences* 23, 251–285.
- Pearce, J.A., Vander Laan, S.R., Arculus, R.J., Murton, B.J., Ishii, T., Peate, D.W., Parkinson, I.J., 1992. Boninite and harzburgite from Leg 125 (Bonin–Mariana forearc): a case study of magma genesis during the initial stages of subduction, in Fryer. Proceeding of the Ocean Drilling Program Scientific Results 125, 623–659.
- Peate, D.W., Hawkesworth, C.J., Marta, M.S.M., Nick, W.R., Turner, S.P., 1999. Petrogenesis and stratigraphy of the high-Ti/Y Urubici magma type in the Parana Flood Basalt Province and implications for the nature of Dupal-type mantle in the South Atlantic region. *Journal of Petrology* 40, 451–473.
- Perfit, M.R., Gust, D.A., Bence, A.E., Arculus, R.J., Taylor, S.R., 1980. Chemical characteristics of Island-arc basalts: implications for mantle sources. *Chemical Geology* 30, 227–256.
- Plank, T., Kelley, K.A., Zimmer, M.M., Hauri, E.H., Wallace, P.J., 2013. Why do mafic arc magmas contain ~4% water on average? *Earth and Planetary Science Letters* 364, 168–179.
- Plank, T., Langmuir, C.H., 1993. The chemical composition of subducting sediment and its consequences for the crust and mantle. *Chemical Geology* 145, 325–384.
- Plank, T., Langmuir, C.H., 1998. The chemical composition of subducting sediments and its consequences for the crust and mantle. *Chemical Geology* 145, 325–394.
- Plank, T., Ludden, J.N., 1992. Geochemistry of sediments in the Argo Abyssal Plain at Site 765: a continental margin reference section for sediment recycling in subduction zones. *Proceedings of the Ocean Drilling Program, Scientific Results* 123, 167–189.
- Polat, A., 2012. Growth of Archean continental crust in oceanic island arcs. *Geology* 40, 383–384.
- Ray, J., Saha, A., Koeberl, C., Thoni, M., Ganguly, S., Hazra, S., 2013. Geochemistry and petrogenesis of Proterozoic mafic rocks from east Khasi Hills, Shillong Plateau, northeastern India. *Precambrian Research* 230, 119–137.
- Reichow, M.K., Saunders, A.D., White, R.V., Al'Mukhamedov, A.I., Medvedev, A.Y., 2005. Geochemistry and petrogenesis of basalts from the West Siberian Basin: an extension of the Permo–Triassic Siberian Traps, Russia. *Lithos* 79, 425–452.
- Rollinson, H.R., 1993. Using Geochemical Data: Evaluation, Presentation, Interpretation. John Wiley, Chichester, p. 352.
- Rudnick, R.L., Gao, S., 2003. Composition of the continental crust. In: Kusky, T.M. (Ed.), *Precambrian Ophiolites and Related Rocks*. Elsevier, Amsterdam, pp. 1–64.
- Rudnick, R.L., Ireland, T.R., Gehrels, G., Irving, A.J., Chesley, J.T., Hanchar, J.M., 1999. Dating Mantle Metasomatism: U–Pb Geochronology of Zircons in Cratonic Mantle Xenoliths from Montana and Tanzania (The P.H. Nixon Volume, Proceedings of the VIIth International Kimberlite Conference).
- Saal, A.E., Hauri, E.H., Langmuir, C.H., Perfit, M.R., 2002. Vapour undersaturation in primitive mid oceanic ridge basalt and the volatile content of Earth's upper mantle. *Nature* 419, 451–455.
- Saccani, E., Beccaluva, L., Coltorti, M., Siena, F., 2004. Petrogenesis and tectonomagmatic significance of the Albanide–Hellenide Subpelagonian ophiolites. *Ophioliti* 29, 77–95.
- Saccani, E., Beccaluva, L., Photiades, A., Zeda, O., 2011. Petrogenesis and tectonomagmatic significance of basalts and mantle peridotites from the Albanian–Greek ophiolites and sub-ophiolitic mélange. New constraints for the Triassic–Jurassic evolution of the Neo-Tethys in the Dinaride sector. *Lithos* 124, 227–242.
- Safonova, I.Yu., 2009. Intraplate magmatism and oceanic plate stratigraphy of the Paleo-Asian and Paleo-Pacific Oceans from 600 to 140 Ma. *Ore Geology Reviews* 35, 137–154.
- Safonova, I.Yu., Simonov, V.A., Buslov, M.M., Ota, T., Maruyama, Sh., 2008. Neo-proterozoic basalts of the Paleo-Asian Ocean (Kurai accretion zone, Gorni Altai, Russia): geochemistry, petrogenesis, geodynamics. *Russian Geology and Geophysics* 49, 254–271.
- Saha, A., Manikyamba, C., Santosh, M., Ganguly, S., Khelen, A.C., Subramanyam, K.S.V., 2015. Platinum Group Elements (PGE) geochemistry of komatiites and boninites from Dharwar Craton, India: implications for mantle melting processes. *Journal of Asian Earth Sciences* 105, 300–319.
- Saha, A., Ganguly, S., Ray, J., Koeberl, C., Thöni, M., Sarbjana, C., Sawant, S.S., 2017. Petrogenetic evolution of Cretaceous Samchampi–Samteran Alkaline Complex, Mikir Hills, Northeastern India: implications on multiple melting events of heterogeneous plume and metasomatized sub-continental lithospheric mantle. *Gondwana Research* 48, 237–256.
- Sajona, F.G., Maury, R.C., Bellon, H., Cotton, J., Defant, M., 1996. High field strength element enrichment of Pliocene–Pleistocene island arc basalts, Zamboanga Peninsula, western Mindanao (Philippines). *Journal of Petrology* 37, 693–726.
- Santosh, M., 1987. Cordierite gneisses of southern Kerala, India: petrology, fluid inclusions and implications for crustal uplift history. *Contributions to Mineralogy and Petrology* 96, 343–356.
- Santosh, M., 2010. Supercontinent tectonics and biogeochemical cycle: a matter of ‘life and death’. *Geoscience Frontiers* 1, 21–30.
- Santosh, M., 2013. Evolution of continents, cratons and supercontinents: building the habitable Earth. *Current Science* 104, 871–879.
- Santosh, M., Maruyama, S., Sato, K., 2009. Anatomy of a Cambrian suture in Gondwana: Pacific-type orogeny in southern India. *Gondwana Research* 16, 321–341.
- Santosh, M., Liu, D., Shi, Y., Liu, S.J., 2013. Paleoproterozoic accretionary orogenesis in the North China Craton: a SHRIMP zircon study. *Precambrian Research* 227, 29–54.
- Santosh, M., Morimoto, T., Tsutsumi, Y., 2006. Geochronology of the khondalite belt of Trivandrum Block, southern India: electron probe ages and implications for Gondwana tectonics. *Gondwana Research* 9, 261–278.
- Santosh, M., Tsunogae, T., Malavariarachchi, S.P.K., Zhang, Z., Ding, H., Tang, L., Dharmapriya, P.L., 2014. Neoproterozoic crustal evolution in Sri Lanka: Insights from petrologic, geochemical and zircon U–Pb and Lu–Hf isotopic data and implications for Gondwana assembly. *Precambrian Research* 255, 1–29.
- Santosh, M., Yang, Q.Y., Shaji, E., Ram Mohan, M., Tsunogae, T., Satyanarayanan, M., 2016. Oldest rocks from Peninsular India: evidence for Hadean to Neoproterozoic crustal evolution. *Gondwana Research* 29, 105–135.
- Santosh, M., Yang, Q.Y., Shaji, E., Tsunogae, T., Mohan, M.R., Satyanarayanan, M., 2015. An exotic Mesoarchean microcontinent: the Coorg Block, southern India. *Gondwana Research* 27, 165–195.
- Santosh, M., Yokoyama, K., Sekhar, S.B., Rogers, J.J.W., 2003. Multiple tectono-thermal events in the Granulite Block of Southern India revealed from EPMA dating: implications on the history of supercontinents. *Gondwana Research* 6, 29–63.
- Santosh, M., Hu, C.N., He, X.F., Li, S.S., Tsunogae, T., Shaji, E., Indu, G., 2017. Neoproterozoic arc magmatism in the southern Madurai Block, India: subduction, relamination, continental outbuilding, and the growth of Gondwana. *Gondwana Research* 45, 1–42.
- Sato, M., Shuto, K., Uematsu, M., Takahashi, T., Ayabe, M., Takanashi, K., Ishimoto, H., Kawabata, H., 2013. Origin of Late Oligocene to Middle Miocene adakitic andesites, high magnesian andesites and basalts from the back-arc margin of the SW and NE Japan arcs. *Journal of Petrology* 54, 481–524.
- Satyanarayanan, M., Balaram, V., Sawant, S.S., Subramanyam, K.S.V., Krishna, G.V., 2014. High precision multielement analysis on geological samples by HR-ICP-MS. In: Aggarwal, S.K., Jaisan, P.G., Sarkar, A. (Eds.), *28th ISMAS Symposium and Workshop on Mass Spectrometry ISMAS Secretariat*, Mumbai, pp. 181–184.
- Saunders, A.D., Norry, M.J., Tarney, J., 1988. Origin of MORB and chemically-depleted mantle reservoirs: trace element constraints. *Journal of Petrology* (Special Lithosphere Issue) 415–445.
- Saunders, A.D., Storey, M., Kent, R.W., Norry, M.J., 1992. Consequences of plume–lithosphere interactions. In: Storey, B.C., Alabaster, T., Pankhurst, R.J. (Eds.), *Magma and the Causes of Continental Breakup*, Geological Society of London Special Publication, vol. 68, pp. 41–60.
- Saunders, A.D., Tarney, J., Weaver, J., 1980. Transverse geochemical variations across the Antarctic Peninsula: implications for the genesis of calc-alkaline magmas. *Earth and Planetary Science Letters* 46, 344–360.
- Schuth, S., Munker, C., Konig, S., Opoto, C., Basi, S., Garbe-Schonberg, D., Ballhaus, C., 2009. Petrogenesis of lavas along the Solomon Island Arc, SW Pacific: coupling of compositional variations and subduction zone geometry. *Journal of Petrology* 50, 781–811.
- Shellnutt, J.G., Bhat, G.M., Wang, K., Brookfield, M.E., Jahn, B., Dostal, J., 2014. Petrogenesis of the flood basalts from the Early Permian Panjal Traps, Kashmir, India: geochemical evidence for shallow melting of the mantle. *Lithos* 204, 159–171.
- Sheraton, J.W., Black, L.P., McCulloch, M.T., Oliver, R.L., 1990. Age and origin of a compositionally varied mafic dyke swarm in the Bungur Hills, East Antarctica. *Chemical Geology* 85, 215–246.

- Shuto, K., Sato, M., Kawabata, H., Osanai, Y., Nakano, N., Yashima, R., 2013. Petrogenesis of Middle Miocene Primitive Basalt, andesite and garnet-bearing adakitic rhyodacite from the Ryozen Formation: implications for the tectono-magmatic evolution of the NE Japan Arc. *Journal of Petrology* 54, 2413–2454.
- Skiyarov, E.V., Gladkochub, D.P., Mazukabzov, A.M., Menshagin, Y.V., Watanabe, T., Pisarevsky, S.A., 2003. Neoproterozoic mafic dike swarms of the Sharyzhalgai metamorphic massif, southern Siberian craton. *Precambrian Research* 122, 359–376.
- Song, X.-Y., Qi, H.-W., Robinson, P.T., Zhou, M.-F., Cao, Z.-M., Chen, L.-M., 2008. Melting of the subcontinental lithospheric mantle by the Emeishan mantle plume; evidence from the basal alkaline basalts in Dongchuan, Yunan, Southwestern China. *Lithos* 100, 93–111.
- Song, X.-Y., Zhou, M.-F., Hou, Z.-Q., Cao, Z.-M., Wang, Y.-L., Li, Y., 2001. Geochemical constraints on the mantle source of the Upper Permian Emeishan Continental Flood Basalts, Southwestern China. *International Geology Review* 43, 213–225.
- Song, X.-Y., Zhou, M.-F., Keays, R.R., Cao, Z.-M., Sun, M., Qi, L., 2006. Geochemistry of the Emeishan flood basalts at Yangtziplung, Sichuan, SW China: implications for sulphide segregation. *Contributions to Mineralogy and Petrology* 152, 53–74.
- Spencer, C.J., Kirkland, C.L., Taylor, R.J.M., 2016. Strategies towards statistically robust interpretations of in situ U-Pb zircon geochronology. *Geoscience Frontiers* 7 (4), 581–589.
- Spencer, C.J., Yakymchuk, C., Ghaznavi, M., 2017. Visualising data distributions with kernel density estimation and reduced chi-squared statistic. *Geoscience Frontiers* 8 (6), 1247–1252.
- Stern, R.J., Morris, J., Bloomer, S.H., Hawkins Jr., J.W., 1991. The source of metasomatic fluids and the generation of arc melts: trace element and radiogenic isotope evidence from Eocene boninites, Mariana forearc. *Geochimica et Cosmochimica Acta* 55, 1467–1481.
- Stern, R.J., 2002. Subduction zones. *Reviews of Geophysics* 40 (4), 3–1–3–38.
- Sun, S.S., Mc Donough, W.F., 1989. Chemical and isotopic systematics of oceanic basalts, implications for mantle composition and processes. In: Saunders, A.D., Norry, M.J. (Eds.), *Magmatism in the Ocean Basins*, Geological Society of London Special Publication, vol. 42. Blackwell Scientific Publication, UK, pp. 313–345.
- Sweeney, R.J., Duncan, A.R., Erlank, A.J., 1994. Geochemistry and petrogenesis of central Lebombo basalts of the Karoo igneous province. *Journal of Petrology* 35, 95–125.
- Sylvester, P.J., Campbell, I.H., Bowyer, D.A., 1997. Niobium/uranium evidence for early formation of continental crust. *Science* 275, 521–523.
- Tatsumi, Y., 2005. The subduction factory: how it operates in the evolving Earth. *Geological Society of America Today* 15, 4–10.
- Taylor, S.R., McLennan, S.M., 1985. *The Continental Crust: Its Composition and Evolution*. Blackwell, Oxford, p. 312.
- Thompson, R.N., Morrison, M.A., Hendry, G.L., Parry, S.J., 1984. An assessment of the relative roles of crust and mantle in magma genesis: an elemental approach. *Philosophical Transactions of the Royal Society of London A310*, 549–590.
- Volker, D., Wehrmann, H., Kutterolf, S., Iyer, K., Rabbel, W., Geersen, J., Hoernle, K., 2014. Contrasting input and output fluxes of southern-central Chile subduction zone: water, chlorine and sulphur. *International Journal of Earth Science* 103 (7), 2129–2153.
- Walter, M.J., 1998. Melting of garnet peridotite and the origin of komatiite and depleted lithosphere. *Journal of Petrology* 39, 29–60.
- Wilson, M., 1989. *Igneous Petrogenesis*. Unwin Hyman, London, p. 466.
- Woodhead, J.D., Herdt, J.M., Davidson, J.P., Egginis, S.M., 2001. Hafnium isotope evidence for ‘conservative’ element mobility during subduction zone processes. *Earth and Planetary Science Letters* 192, 331–346.
- Woodhead, J., Egginis, S., Gamble, J., 1993. High field strength and transition element systematics in island arc and back-arc basin basalts: evidence for multi-phase melt extraction and a depleted mantle wedge. *Earth and Planetary Science Letters* 114, 491–504.
- Xiong, X., Keppler, H., Audetat, A., Ni, H., Sun, W., Li, Y., 2011. Partitioning of Nb and Ta between rutile and felsic melt and the fractionation of Nb/Ta during partial melting of hydrous metabasalt. *Geochimica et Cosmochimica Acta* 75, 1673–1692.
- Xu, Y.-G., Ma, J.-L., Frey, F.A., Feigenson, M.D., Liu, J.-F., 2005. Role of lithosphere–asthenosphere interaction in the genesis of Quaternary alkali and tholeiitic basalts from Datong, western North China Craton. *Chemical Geology* 224 (4), 247–271.
- Yang, Q.Y., Santosh, M., Ganguly, S., Arun-Gokul, J., Dhanil Dev, S.G., Tsunogae, T., Shaji, E., Dong, Y., Manikyamba, C., 2016b. Melt-fluid infiltration in Archean suprasubduction zone mantle wedge: evidence from geochemistry, zircon U-Pb geochronology and Lu-Hf isotopes from Wynad, southern India. *Precambrian Research* 281, 101–127.
- Yang, Q.Y., Santosh, M., Maruyama, S., Nakagawa, M., 2016a. Proto-Japan and tectonic erosion: evidence from zircon geochronology of blueschist and serpentinite. *Lithosphere* 8, 386–395.
- Yang, W.B., Niu, H.C., Shan, Q., Chen, H.Y., Hollings, P., Li, N.B., Yan, S., Zartman, R.E., 2014. Geochemistry of primary-carbonate bearing K-rich igneous rocks in the Awulale Mountains, western Tianshan: implications for carbon-recycling in subduction zone. *Geochimica et Cosmochimica Acta* 143, 143–164.
- Yaxley, G.M., 2000. Experimental study of the phase and melting relations of homogeneous basalt+peridotite mixtures and implications for the petrogenesis of flood basalts. *Contributions to Mineralogy and Petrology* 139, 326–338.
- Yogodzinski, G.M., Kay, R.W., Volynets, O.N., Koloskov, A.V., Kay, S.M., 1995. Magnesian andesite in the western Aleutian Komandorsky region: implications for slab melting and processes in the mantle wedge. *The Geological Society of America Bulletin* 107, 505–519.
- Yuan, H.L., Gao, S., Liu, X.M., Li, H.M., Gunther, D., Wu, F.Y., 2004. Accurate U-Pb age and trace element determinations of zircon by laser ablation–inductively coupled plasma mass spectrometry. *Geostandards Newsletter* 28, 353–370.
- Zhao, J.J., Zhou, M.F., 2007. Geochemistry of Neoproterozoic mafic intrusions in the Panzhihua district (Sichuan Province, SW China): implications for subduction related metasomatism in the upper mantle. *Precambrian Research* 152, 27–47.
- Zhao, J.-X., Shiraishi, K., Ellis, D.J., Sheraton, J.W., 1995. Geochemical and isotopic studies of syenites from the Yamato Mountains, East Antarctica: implications for the origin of syenitic magmas. *Geochimica et Cosmochimica Acta* 59, 1363–1382.